

## Onset of the anorogenic alkaline magmatism in the Nigerian Younger Granite province: Constraints from the Daura and Dutse complexes

Victor Ikechukwu Vincent<sup>a</sup>, Lian-Xun Wang<sup>a,b,\*</sup>, Yu-Xiang Zhu<sup>a</sup>, Vandi Dlama Kamaunji<sup>a</sup>, Hafizullah Abba Ahmed<sup>c</sup>, Eyo Eyo Ntekim<sup>c</sup>, Liang Cao<sup>b,d</sup>

<sup>a</sup> School of Earth Sciences, China University of Geosciences, 430074 Wuhan, PR China

<sup>b</sup> Research Center for Petrogenesis and Mineralization of Granitoid Rocks, CGS, 430205 Wuhan, China

<sup>c</sup> Department of Geology, Modibbo Adama University of Technology, P.M.B. 2076, Yola, Nigeria

<sup>d</sup> Wuhan Center of Geological Survey, CGS, 430205 Wuhan, China

### ARTICLE INFO

#### Keywords:

Anorogenic alkaline magmatism  
A<sub>1</sub>-type granite  
Daura and Dutse complex  
Nigeria  
Younger granites

### ABSTRACT

The Younger Granite province of Niger and Nigeria exemplifies a classical anorogenic alkaline ring granite belt with southward age migration from ca. 470 Ma to 140 Ma. However, the precise age transition from the older Nigerien Younger Granite (NrYG) to the younger Nigerian Younger Granite (NaYG) is poorly constrained. The Daura and Dutse complexes, located at the northernmost tip of the NaYG province, represent a temporal and spatial link between the NrYG and NaYG provinces. The Daura complex is composed of amphibole syenite and biotite granite, while the Dutse complex consists of fayalite syenite and arfvedsonite aegirine granite. Similar to other alkaline rocks of the NrYG and NaYG provinces, the Daura and Dutse samples all chemically show typical A<sub>1</sub>-type granite features, such as high alkalis ( $K_2O + N_2O = 8.33\text{--}11.27$  wt%), Ga/Al ratios, Zr + Nb + Ce + Y contents (527–2345 ppm) and FeOt/(FeOt + MgO) ratios (0.03–0.70) as well as elevated HFSEs. The Nd—Hf and Pb isotopic systematics show that all the syenite-granites yield  $\epsilon_{Nd}(t) = -2.9$  to +1.5,  $\epsilon_{Hf}(t) = -3.8$  to +16.7, and  $^{206}\text{Pb}/^{204}\text{Pb} = 17.818$  to 19.555, suggestive of magmas derived from a slightly depleted mantle source with OIB imprints. A reduced to slightly oxidized redox state is invoked for the parental melt based on estimations from mineral chemistry. The Daura amphibole syenite is composed of >60% alkali feldspar, show high Eu/Eu\* (>1), Ba/Zr (>3.5) values and cumulate textures, resembling an alkali feldspar cumulate rock. The other alkaline granitic rocks were likely generated from variable fractional crystallization of the residual melt with distinct crustal contaminations. Zircon U—Pb dating reveal that the Daura amphibole syenite and biotite granite were emplaced at  $324 \pm 1$  Ma and  $321 \pm 3$  Ma, respectively, whereas the Dutse granitoids showed episodic intrusive periods of ca. 264 Ma and 232 Ma. All these results predate other anorogenic alkaline complexes of the NaYG and update the oldest age (ca. 214 Ma in previous references) recorded in the alkaline granite province. To the north, it connects well with ages from the Zinder complex (~330 Ma) in the southernmost NrYG province, reflecting a significant link between the NrYG and NaYG provinces. From a broad view, a linear age migration from north to south in the Niger-Nigeria Younger Granite province remains well preserved, although temporal and spatial intervals exist in local region. This emplacement pattern can be traced to the periodic and repeated reactivation of lithospheric shear zones and transcurrent faults.

### 1. Introduction

Temporospatial distribution of alkaline magmatism is typically linked to either deep-rooted thermal anomalies (plumes: SW Portugal – Grange et al., 2010) or shear-driven melt upwelling (SW French Polynesia – Ballmer et al., 2013). In Africa, continuous alkaline/volcanic chains are found across the Niger-Nigeria-Cameroon alkaline belt (West

Africa) and the East African Rift system. The West African alkaline belt represents continuous magmatism unrelated to orogenic events (Halliday et al., 1988), while the East African rift represents an active continental rift system (Ebinger, 2005). In the West African alkaline belt, the Niger-Nigeria alkaline granite province exemplifies a classic example of within plate age migration of magmatic centres across a vast region (1300 km long; Black et al., 1985; Ngako et al., 2006). A general

\* Corresponding author at: School of Earth Sciences, China University of Geosciences, 430074 Wuhan, PR China.  
E-mail address: [lianxunwang@cug.edu.cn](mailto:lianxunwang@cug.edu.cn) (L.-X. Wang).

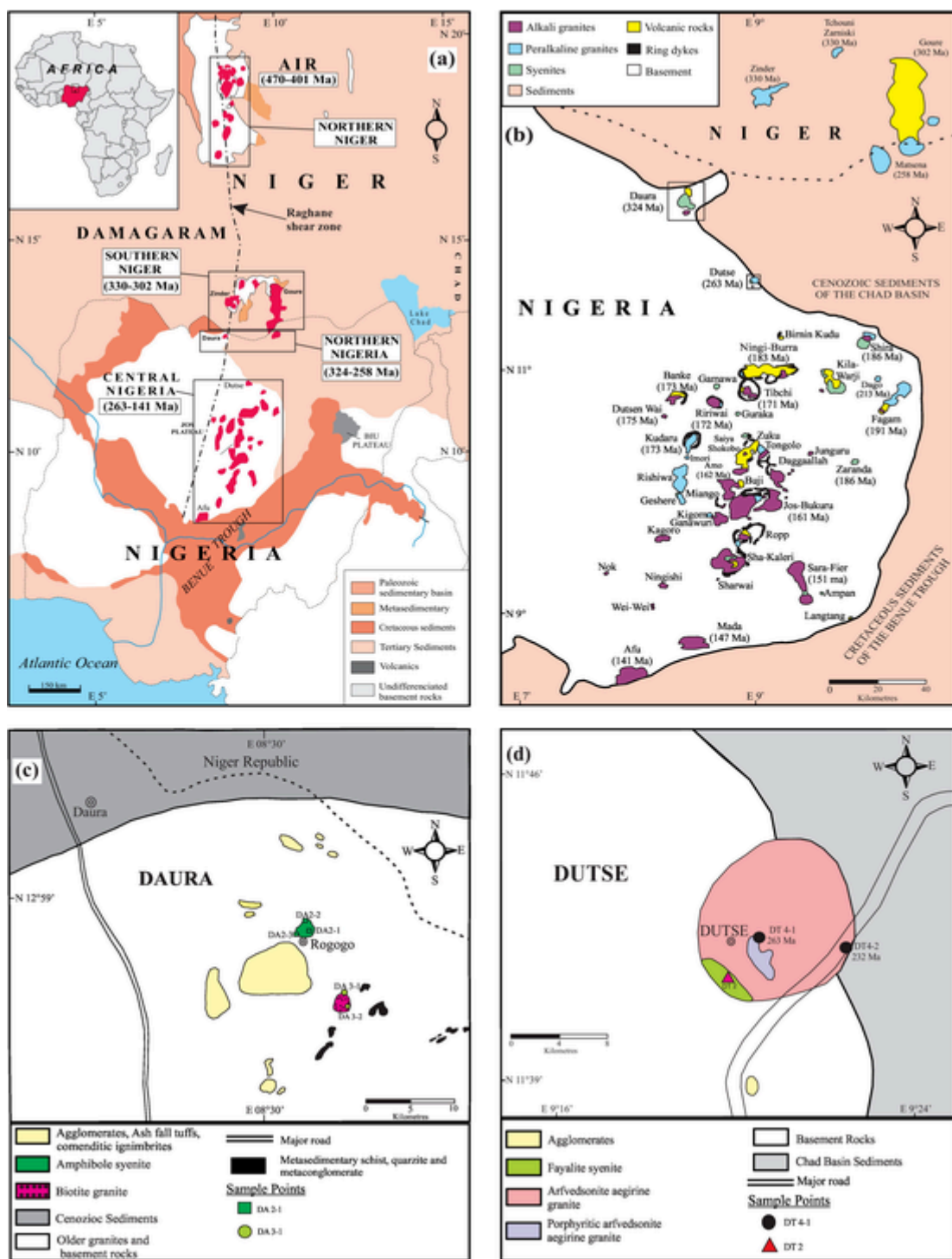


**Fig. 1.** (a) Distribution map of alkaline ring complexes in the West African Craton (WAC), (b) Schematic map showing the distribution of alkaline intrusive complexes in the Nigerian Younger Granite Field. Rb—Sr age data taken from Rahaman et al. (1984). Modified from Kinnaid (1981), (c) Geologic Map of the Daura Complex, and (d) Geologic map of the Dutse complex (modified after Turner and Webb, 1974).

N-S decreasing age trend has been traced for the alkaline suites of the Niger-Nigeria alkaline granite province (Rahaman et al., 1984; Van Breemen and Bowden, 1973). Several models including mantle plume theory (Bowden et al., 1976; Kamaunji et al., 2020), reactivated transtensional fault system (Rahaman et al., 1984), and complex interplay between mantle plume and ancient lineament (Ngako et al., 2006) have been proposed to explain the N-S decreasing age patterns in the Niger-Nigeria alkaline belt. However, more precise geochronological work, detailed mineralogical and petrological investigation applying new an-

alytical techniques are required to provide robust evidence for the appropriate geodynamic model.

Since the Nigerian alkaline-peralkaline granites were first recognized as “A-type” suites by Loiselle and Wones (1979) and characterized as a typical location of within-plate granites (WPG) by Eby (1990), debate has persisted regarding their specific origins and the genetic relationships. Some recent studies involving whole rock Sr-Nd-Pb and in situ zircon Hf isotope systematics portray the Nigerian A-type granites as sourced from basaltic mantle magmas with crustal involvement (e.g.,

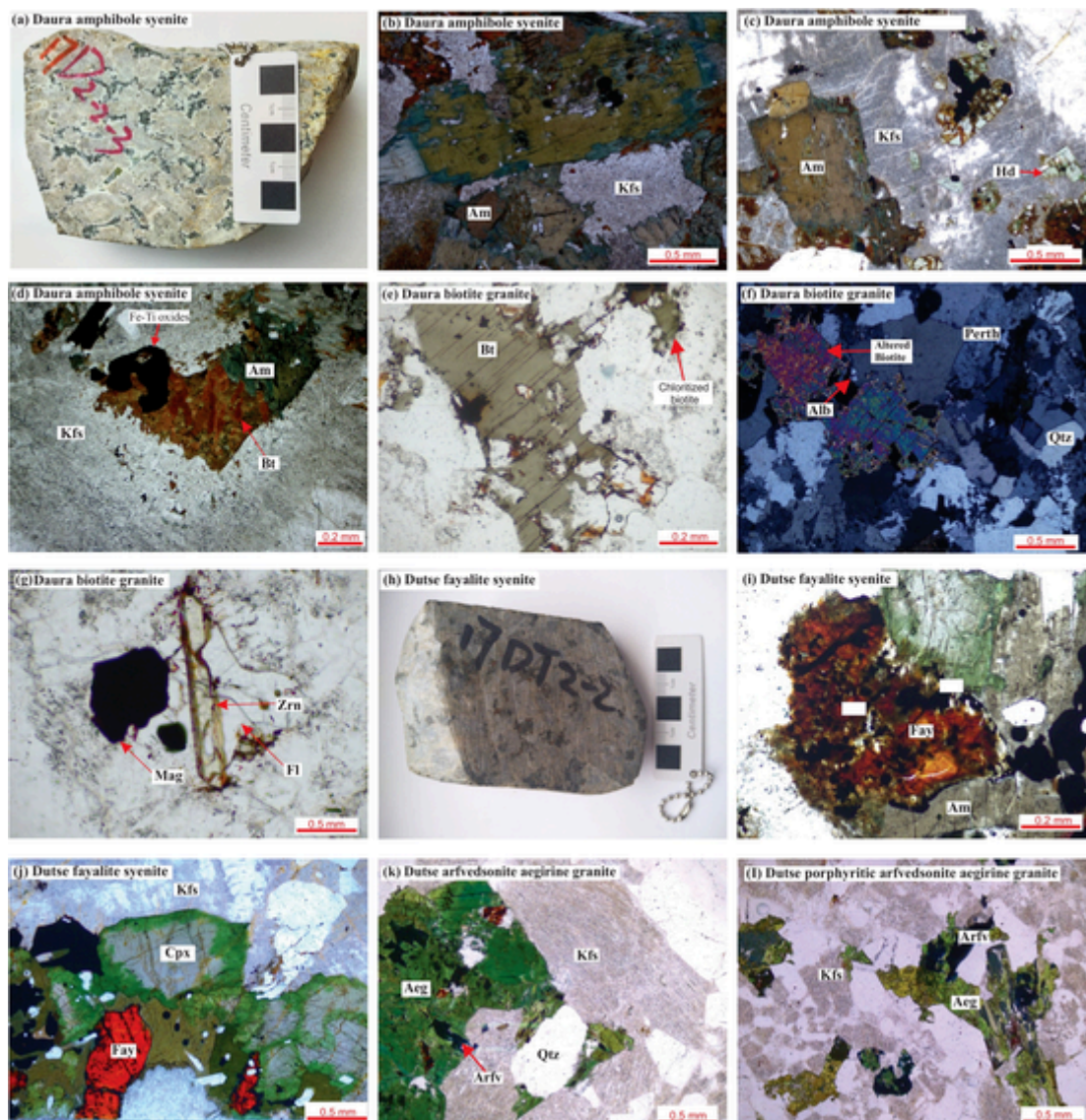


**Fig. 2.** (a) Hand specimen microphotograph of the Daura fayalite syenite; Thin section microphotograph of (b–d) the Daura syenite; (e–g) the Daura biotite granite; (h) Hand specimen microphotograph of the Daura fayalite syenite; (i–j) Thin section microphotograph of the Dutse fayalite syenite; (k) the Dutse arfvedsonite aegirine granite and (l) the Dutse arfvedsonite aegirine granite (porphyritic variety). Abbreviations: Ab, albite; Aeg, aegirine; Amp, Amphibole; Arf, Arfvedsonite; Bt, biotite; Cpx, Clinopyroxene; Fa, Fayalite; Fl, Flourine; Hd, Hedenbergite; Kfs: K-feldspar; Mag, Magnetite; Perth, perthite; Qtz, quartz; Zrn: Zircon.

Ahmed et al., 2021; Amuda et al., 2020; Girei et al., 2019; Kamaunji et al., 2020). By contrast, considering the less radiogenic Sr—Nd and Hf isotopic compositions and oxidized nature of the Mo-mineralized aluminous biotite granites in Mada, Girei et al. (2020) proposed a lower crustal origin with contributions from the upper mantle. Similarly, Magaji et al. (2011) advocated an alkali-metasomatized and fenitized lower crustal origin for the Nigerian alkaline-peralkaline granites. However, the less radiogenic crustal-like  $\epsilon$ Nd (t) isotopic compositions reported for the Kudaru biotite granite has been ascribed to crustal contamination rather than derivation from a pure crustal source (e.g., Kamaunji et al., 2020).

The Daura and Dutse complexes are parts of the large anorogenic alkaline granite province in northcentral Nigeria (also known as the Nigerian Younger Granite, NaYG) with more than 50 Mesozoic alkaline complexes covering an area of about 75,000 km<sup>2</sup> (Bowden et al., 1987; Kinnaird, 1985). The Daura and Dutse complexes link the migrating belts of Paleozoic and Mesozoic alkaline complexes in Niger and Nigeria (Rahaman et al., 1984; Turner and Webb, 1974), given their location across the Niger-Nigeria boundary (Fig. 1b). Thus, these two alka-

line complexes have been considered as the earliest manifestation of post-Cambrian alkaline magmatism in Nigeria (Kinnaird, 1981). However, due to limited studies (Bennett et al., 1984; Turner and Webb, 1974), the precise geochronology and petrogenesis of the two complexes are poorly understood. Although an imprecise Rb—Sr age has been reported for the Daura complex (~307 Ma; Rahaman et al., 1984), a much younger age of 213 Ma for the Dutse complex (Rahaman et al., 1984) has been widely used as the onset time of the post-Cambrian alkaline magmatism in the NaYG province (Girei et al., 2019; Kamaunji et al., 2020). The lack of precise geochronological data also hindered detailed reconstruction of structural controls on the distribution of the NaYG alkaline complexes and age migration trends for the Nigerian alkaline granite province (Dickin et al., 1991; Rahaman et al., 1984).

Herein, a combined study of whole-rock major and trace elements, mineral chemistry, zircon U—Pb dating and Lu—Hf isotopes, as well as whole-rock Nd—Pb isotopic systematics on the Daura-Dutse granitoids is presented. The primary aim is to constrain precise intrusive ages, the origin and genetic relationship of the diverse granitoid suites

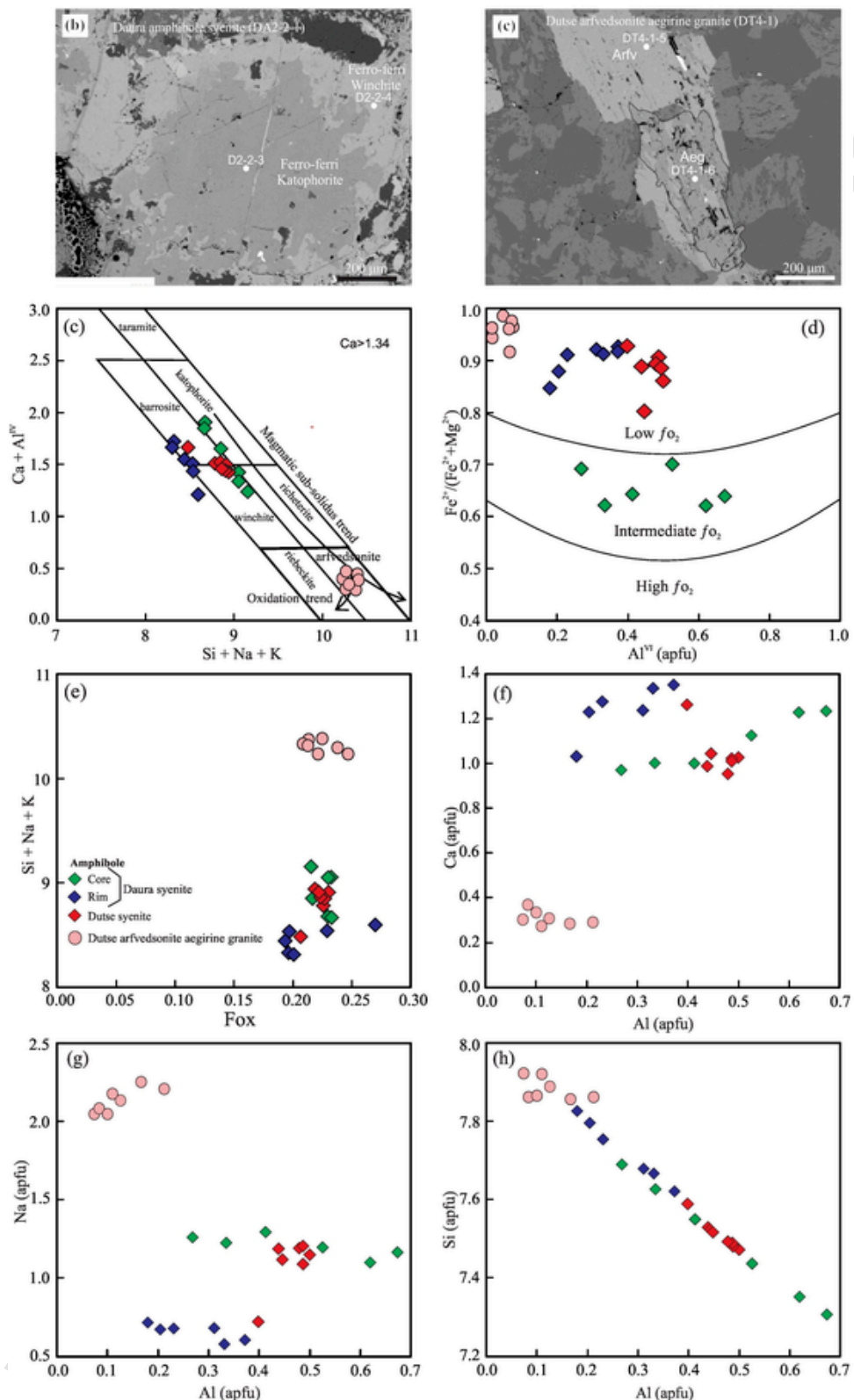


**Fig. 3.** Plots of amphiboles from the Daura and Dutse complex. (a–b) BSE images of arfvedsonite grains from the Daura amphibole syenite showing evidence of zonation, (c)  $\text{Si} + \text{Na} + \text{K}$  vs.  $\text{Al}^{\text{IV}} + \text{Ca}$  diagram, (d)  $\text{Fe}^{2+}/(\text{Fe}^{2+} + \text{Mg}^{2+})$  vs.  $\text{Al}^{\text{IV}}$  discrimination diagram, (e) Fox vs.  $\text{Si} + \text{Na} + \text{K}$  diagram. Binary diagrams showing major and minor element concentrations of amphibole in atoms per formula unit (apfu), (f) Al vs Ca, (g) Al vs Na, and (h) Al vs Si. The decreasing Al content monitors the differentiation of the magma. Abbreviations: Arfv, Arfvedsonite; Aeg: Aegirine.

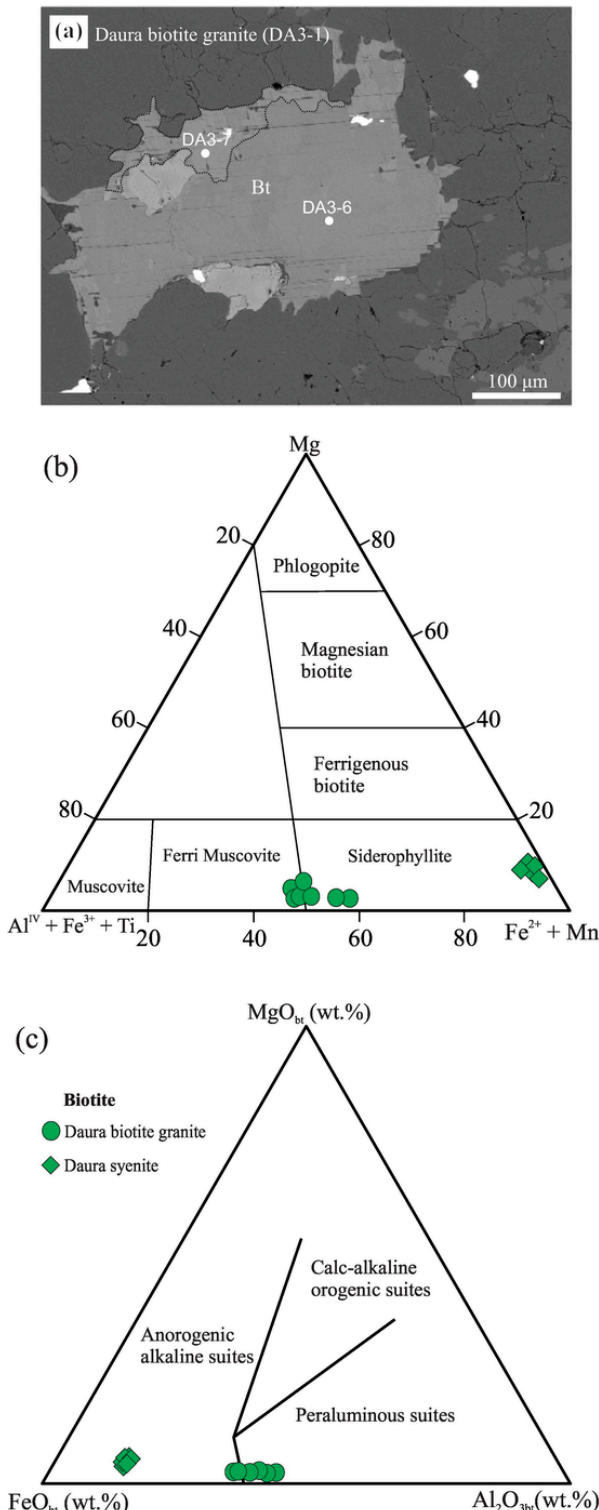


**Fig. 4.** (a) Representative BSE images and chemical plots of biotite grains from the Daura biotite granite. (b) Ternary  $Mg-Al^{VI} + Fe^{3+} + Ti-Fe^{2+} + Mn$ , and (c) Ternary  $MgO-FeO-Al_2O_3$  diagram. Abbreviations: Bt, biotite.

(syenite-granite) found in both the Daura and Dutse complexes. The new dataset will also shed new light on the geodynamic model from which the Niger-Nigeria alkaline granite province were formed.

## 2. Geologic setting and sample description

### 2.1. Niger-Nigeria alkaline granite province

The Niger-Nigeria alkaline granite province comprises about 80 anorogenic alkaline complexes of Paleozoic to Mesozoic age (Fig. 1a, b). These complexes occur in four distinct centres namely: Air Massif (northern Niger), Zinder-Mounio Centre (southern Niger), Daura-Matsena Centre (northern Nigeria) and Jos Plateau Centre (northcentral Nigeria). Over 50 complexes occur within Nigeria, and around 24 others are found in Niger (Black et al., 1985; Kinnaird, 1985). These alkaline complexes were emplaced within the Precambrian basement, which are remnants of the Eburnean orogeny and are mainly cross-cut by Neoproterozoic Pan-African granitoids (Bute et al., 2019). According to previous Rb—Sr dating results, a southward age migration sequence (older to younger) for the high-level alkaline complexes of the Niger-Nigeria province is apparent (Bowden et al., 1987). The four distinct centres harbor similar anorogenic complexes with common associations of syenite and granitoids; however, slight differences are present in terms of their volumetric proportions (Black et al., 1985; Girei et al., 2019; Kamaunji et al., 2020). The anorogenic complexes of the Air Massif in northern Niger are predominantly alkaline-peralkaline syenite and granites with less abundant metaluminous granites, syenites and feldspar-rich cumulates (DeMaiffe et al., 1991). Ring complexes of the Damagaram-Mounio centre in southern Niger and Daura-Matsena centres of northern Nigeria show variation that is more extensive in composition with almost equal parts of syenite and granite suites (Black et al., 1985). The alkaline complexes in northcentral Nigeria grade from predominantly alkaline-peralkaline suites in the northern sector to metaluminous biotite granitic suites in the southern sector (Kinnaird, 1985).

In Nigeria, the NaYG province covers an area of over 75,000 km<sup>2</sup> within a 400 × 160 km wide N-S trending belt between 8°N and 12°N and longitudes 8°E and 10°E (Fig. 1b; Kinnaird, 1985). Initiation of magma emplacement in the NaYG province is marked by volcanic eruptions of ignimbrite, basalt, rhyolite and trachyte, followed by cauldron collapse and subsequent emplacement of ring dykes. These ring dykes are mostly exemplified in the Nigerian sector as fayalite/pyroxene-bearing granite porphyries representing the first plutonic succession in these complexes (Kamaunji et al., 2020). Emplacement of peralkaline units (prevalent in the northern centres) and metaluminous units (commonplace in the southern centres) marks the main stage of plutonism in the NaYG province. The peralkaline rocks are predominantly arfvedsonite granites, and the metaluminous rocks are mainly biotite granites. Acid-veined mafic rocks, gabbros and syenites make up a minor part of the plutonic units. World-class Sn-Nb-Ta-REE and Pb-Zn-Cu mineralizations have been found throughout the NaYG province, particularly associated with F-rich phases with accompanying sodic, potassic, acid and silica metasomatism of these rocks (Amuda et al., 2020; Girei et al., 2019; Li et al., 2020a; Vonopartis et al., 2021).

### 2.2. The Daura and Dutse complexes

The Daura and Dutse complexes of the northern NaYG province are located close to the Zinder-Mounio complexes of southern Niger (Fig. 1b). The complexes intrude into metasediments of the Kazaure schist belt and Paleoproterozoic basement migmatites and gneisses (Bennett et al., 1984). Ring dykes and cauldron subsidence structures typical of other alkaline granite complexes in the NaYG province are conspicuously absent in the Daura and Dutse alkaline rocks and may represent

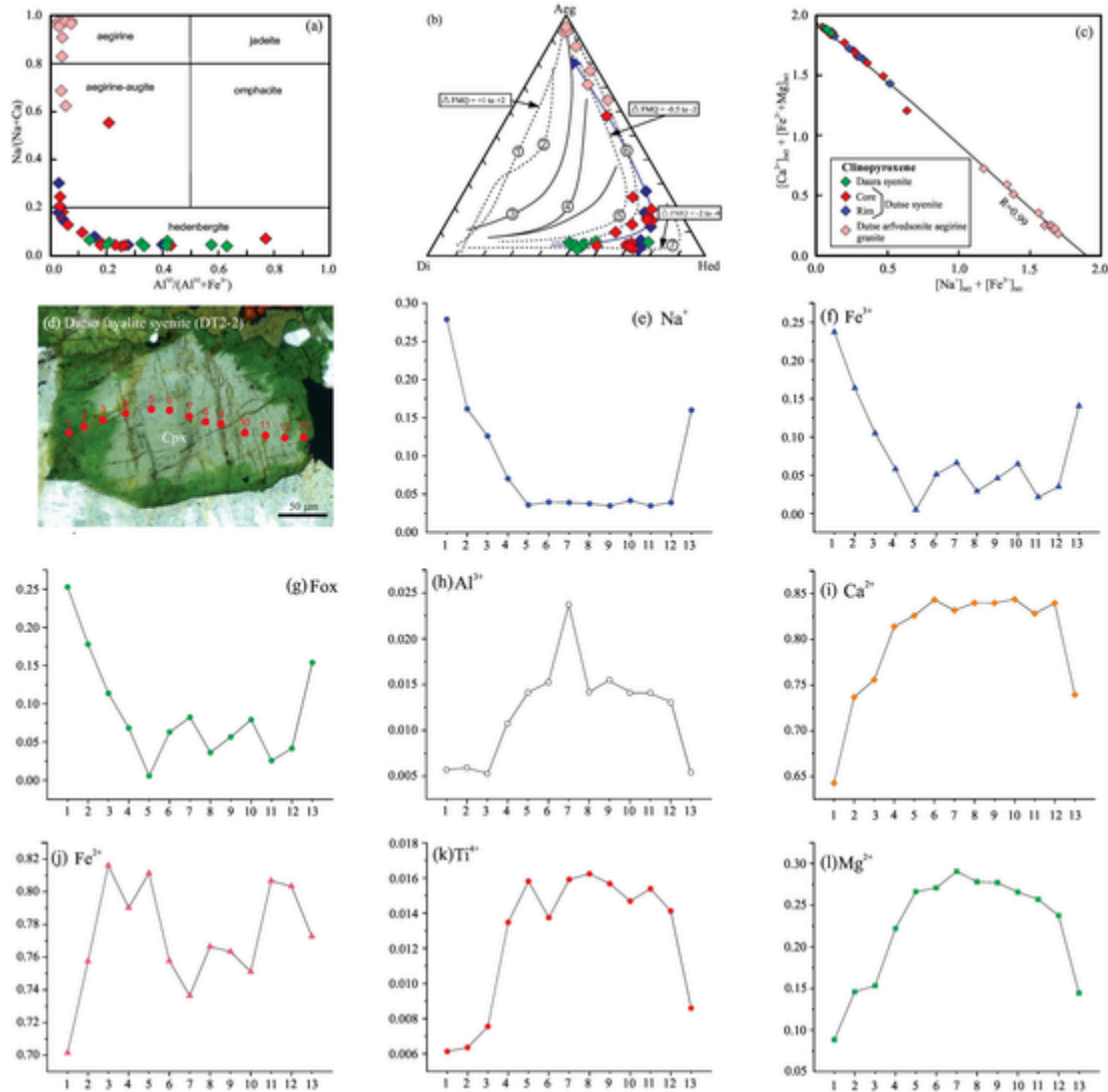


**Fig. 5.** Chemical plots of clinopyroxenes from the Daura and Dutse syenites. (a)  $\text{Al}^{\text{VI}}/(\text{Al}^{\text{VI}} + \text{Fe}^{3+})$  vs.  $\text{Na}/(\text{Na} + \text{Ca})$  diagram (b) Aegirine-diopside-hedenbergite (Aeg-Di-Hed) ternary diagram showing the compositional variation of clinopyroxene. Clinopyroxene evolution trends of 1 - Katzenbuckel, SW Germany; 2 - Murun, Russia; 3 - Lovozero, Russia; 4 - Alno, Sweden; 5 - Coldwell nepheline syenites, Canada; 6 - North Qoroq, South Greenland; 7 - Ilmaussaq, South Greenland are from Marks et al. (2008) and references therein. Quantitative data on oxygen fugacity (given as  $\Delta\text{FMQ}$  units) corresponds to various evolution of clinopyroxene. Blue curve indicates an evolutionary path of clinopyroxene for the syenites, (c)  $(\text{Ca} + \text{Fe}^{2+} + \text{Mn} + \text{Mg})$  vs.  $(\text{Na} + \text{Fe}^{3+})$  diagram for the clinopyroxene in the syenites. Fox =  $\text{Fe}^{3+}/(\text{Fe}^{3+} + \text{Fe}^{2+})$ . Rim–core–rim cationic (apfu) profiles describing the main compositional variations in selected crystals of clinopyroxenes from the Dutse fayalite syenites, (d)  $\text{Al}^{3+}$ , (e)  $\text{Ti}^{4+}$ , (f)  $\text{Mg}^{2+}$ , (g)  $\text{Fe}^{3+}$ , (h) Analytical spots are depicted in a photomicrograph image of the crystal, (i)  $\text{Ca}^{2+}$ , (j)  $\text{Fe}^{2+}$ , (k) Fox, and (l)  $\text{Na}^{+}$ . Bright cores are Ti- and Ca-rich, while dark green rims are Na- and  $\text{Fe}^{3+}$ -rich. Fox =  $\text{Fe}^{3+}/(\text{Fe}^{3+} + \text{Fe}^{2+})$ . (For interpretation of the references to colour in this figure legend, the reader is referred to the web version of this article.)

limited magma volume during the formation of the two complexes (Turner and Webb, 1974).

The Daura complex is composed of several outcrops of rhyolite, granite and syenite dispersed over a  $25 \times 10$  km square area (Fig. 1c). Extrusion of rhyolite marks the beginning of the volcanic phase in the Daura area (Turner and Webb, 1974). Tuff, conglomerate and ignimbrite occur as intercalations within the rhyolite. The plutonic cycle appears to have started by the emplacement of amphibole syenite and then biotite granite. The amphibole syenite found in the central part of the Daura alkaline suites occupies an area of about  $1.5 \text{ km}^2$ . The biotite granite occurs as a single pluton over a  $0.8 \text{ km}^2$  area and is located in the southwestern part of the Daura alkaline complex.

The Dutse complex forms a centric pluton shape and covers an area of over  $40 \text{ km}^2$  (Fig. 1d). It consists of volcanic agglomerate, fayalite syenite and arfvedsonite aegirine granite. A porphyritic and medium-coarse grained variety of the Dutse arfvedsonite aegirine granite (are

construed from field exposures. Extrusion of rhyolite and agglomerate marks the first phase in the Dutse alkaline complex. Previous studies proposed the main plutonic phase began with the emplacement of fayalite syenite as ring dykes followed by the emplacement of the porphyritic arfvedsonite aegirine granite with the medium-coarse grained arfvedsonite aegirine granite representing a later-stage intrusive pluton (Bennett et al., 1984). However, detailed reconstruction of structural features in the field suggest the fayalite syenite and medium-coarse grained arfvedsonite aegirine granite may represent later-staged intrusions into the earlier porphyritic arfvedsonite aegirine granite. The medium-coarse grained arfvedsonite aegirine granite presents as conical massifs occupying an area of around  $28 \text{ km}^2$  and making up over 70% of the total area of the Dutse alkaline suite.

**Table 1**

Major, trace and REE geochemistry for the Daura and Dutse alkaline complexes.

Sample	DA-2-1	DA-2-2	DA-2-3	DA-3-1	DA-3-2	DT4-1	DT4-2	DT2-2
	Amphibole syenite	Amphibole syenite	Amphibole syenite	Biotite granite	Biotite granite	Porphyritic arfvedsonite aegirine granite	Arfvedsonite aegirine granite	Fayalite syenite
Complex	Daura	Daura	Daura	Daura	Daura	Dutse	Dutse	Dutse
<i>Major Element (wt%)</i>								
SiO <sub>2</sub>	61.84	62.47	62.73	77.75	76.81	74.05	71.65	62.9
TiO <sub>2</sub>	0.87	0.68	0.73	0.07	0.07	0.22	0.37	0.64
Al <sub>2</sub> O <sub>3</sub>	15.88	16.31	16.29	12.18	12.26	11.16	11.78	15.64
Fe <sub>2</sub> O <sub>3</sub>	6.66	5.52	5.36	1.38	1.28	3.88	5.01	6.42
MnO	0.19	0.15	0.12	0.02	0.03	0.05	0.10	0.18
MgO	0.70	0.68	0.50	0.05	0.03	0.06	0.08	0.37
CaO	2.12	1.68	1.26	0.3	0.36	0.33	0.59	1.98
Na <sub>2</sub> O	5.98	5.99	5.93	4.78	4.94	4.42	4.85	5.94
K <sub>2</sub> O	5.08	5.28	5.17	3.61	3.39	4.72	4.89	5.04
P <sub>2</sub> O <sub>5</sub>	0.29	0.21	0.23	0.02	0.01	0.01	0.03	0.18
L.O-I	0.51	0.38	0.55	0.45	0.39	0.50	0.40	0.60
D.I.	85	86	87	97	96	90	88	86
A.R	4.19	4.35	4.44	5.10	4.88	8.78	8.41	4.31
Na <sub>2</sub> O + K <sub>2</sub> O	11.06	11.27	11.1	8.39	8.33	9.14	9.74	10.98
K <sub>2</sub> O/Na <sub>2</sub> O	0.85	0.88	0.87	0.76	0.69	1.07	1.01	0.85
A/CNK	0.83	0.88	0.92	0.99	0.98	0.86	0.82	0.83
TZroC	819	817	856	805	805	1008	888	809
<i>Trace elements (ppm)</i>								
Li	10.6	9.1	6.43	122	112	51.8	37.3	6.91
Be	2.56	2.48	2.81	4.47	3.93	12.9	7.13	2.62
Sc	7.30	5.62	9.90	0.33	0.30	2.42	1.11	5.24
V	14.6	10.8	12.5	2.18	2.01	2.30	2.66	4.19
Cr	16.9	13.1	7.4	15.5	14.4	14.3	18.6	7.86
Co	3.12	2.44	1.82	0.60	0.47	0.60	0.89	2.31
Ni	2.50	2.16	1.75	2.19	1.17	1.11	1.67	1.33
Cu	3.97	3.52	2.62	1.71	1.1	2.04	4.19	4.83
Zn	132	117	124	44.8	38.8	247	255	116
Ga	32.7	33	33.4	37.3	36.7	42.3	42.1	36.1
Rb	59.5	66.7	63.2	493	481	208	117	60.1
Sr	185	210	185	9.57	8.13	13	15.9	113
Y	39.8	34.1	48.9	107	99.6	193	145	46.7
Zr	397	346	484	194	197	1624	641	360
Nb	68.5	66.6	78.1	149	136	207	90.5	55.2
Sn	2.53	2.31	2.62	9.35	9.08	19.90	7.38	3.10
Cs	1.05	1.43	1.08	5.04	4.59	0.32	0.78	0.31
Ba	1367	1535	1879	22.9	19.2	74.7	111	806
La	61.8	63.9	70.3	52.9	49.3	196	191	48.1
Ce	128	131	143	102	94.3	321	392	99.9
Pr	15.6	15.0	17.6	10.6	9.88	51.3	53.5	12.6
Nd	63.6	59.6	69.8	34.1	31.6	194	207	52.8
Sm	12.7	11.3	13.8	8.8	8.14	40.2	39.8	11.1
Eu	4.55	4.46	4.87	0.06	0.05	2.10	2.25	4.27
Gd	9.98	8.9	11.8	9.2	8.82	31	34.8	9.83
Tb	1.59	1.36	1.75	2.14	2.01	5.28	5.35	1.61
Dy	8.18	7.30	9.54	15	13.9	31.4	29	9.52
Ho	1.49	1.30	1.74	3.22	3.01	6.40	5.18	1.72
Er	3.97	3.43	4.65	10.2	9.48	19.9	13.4	4.6
Tm	0.55	0.48	0.70	1.72	1.63	3.31	1.84	0.67
Yb	3.39	3.08	4.23	12	11.10	19.80	12.10	4.52
Lu	0.51	0.45	0.60	1.53	1.42	2.69	1.69	0.65
Hf	8.8	8.1	10.4	12.1	13.4	44.5	15	9.79
Ta	3.51	3.6	4.24	11.50	10.20	13.70	3.83	3.30
Tl	0.23	0.22	0.20	1.38	1.34	0.63	0.58	0.16
Pb	9.18	10.4	6.6	16	15.4	55	11.1	4.6
Th	6.83	6.72	8.14	71.1	69.6	41.70	12.80	7.26
U	1.77	1.58	1.99	10.60	14.50	8.61	1.91	1.56
ΣREE	315.49	311.12	354.86	263.65	244.71	924.38	988.91	261.89
(La/Sm)N	3.00	3.49	3.14	3.69	3.73	2.99	2.95	2.67
(La/Yb)N	12.16	13.82	11.07	2.93	2.96	6.60	10.52	7.09
Eu/Eu*	1.25	1.37	1.18	0.02	0.02	0.18	0.19	1.26

(continued on next page)

Table 1 (continued)

Sample	DA-2-2-1	DA-2-2-2	DA-2-2-3	DA-3-1	DA-3-2	DT4-1	DT4-2	DT2-2
	Amphibole syenite	Amphibole syenite	Amphibole syenite	Biotite granite	Biotite granite	Porphyritic arfvedsonite aegirine granite	Arfvedsonite aegirine granite	Fayalite syenite
Complex	Daura	Daura	Daura	Daura	Daura	Dutse	Dutse	Dutse
Nb/U	38.63	42.03	39.27	14.05	9.37	24.04	47.88	35.38
Ba/Zr	3.5	4.4	3.9	0.1	0.1	0.1	0.2	2.2

### 2.3. Petrography

The Daura amphibole syenite is medium to coarse-grained and green to greenish-black in colour (Fig. 2a). Mineralogically (Fig. 2b–c), it is mainly composed of amphibole (10–15%), K-feldspar (55–60 vol%), plagioclase (5–10 vol%), quartz (<5 vol%), biotite (<5 vol%) and hedenbergite (5–10 vol%). Some of the amphibole grains have undergone alteration along the rims forming chlorite halos around fresh grain cores (Fig. 2b). Hedenbergite grains are yellowish green coloured, unzoned and characterized by subhedral to anhedral grains (Fig. 2c). Isolated hedenbergite crystals are subhedral, zoned, and commonly surrounded by K-feldspars and quartz. The biotite grains occur as either irregular or fibrous aggregates intermingling with amphiboles (Fig. 2d). Accessory minerals include apatite, zircon, and Fe—Ti oxides (< 5%).

The Daura biotite granite is mainly fine to medium-grained and grey to yellowish-brown in colour. Feldspar (50–55 vol%), quartz (20–25 vol%) and biotite (5–10 vol%) make up the essential minerals of this rock. Alteration led to significant chloritization of the biotites in some cases (Fig. 2e–f). Quartz commonly occurs as intercalates between perthite and biotite grains (Fig. 2f). Perthite is the dominant alkali feldspar phase in the Daura biotite granite (Fig. 2f). Accessory minerals include fluorite, zircon and magnetite (Fig. 2g).

The Dutse fayalite syenite is medium-grained and greyish to greenish in colour (Fig. 2h). In the thin section, the constituting essential minerals are fayalite (5 vol%), perthitic K-feldspar (55–60 vol%), clinopyroxene (15 vol%), amphibole (15 vol%) and aenigmatite (~5 vol%) with zircon, apatite, titanite and magnetite occurring as essential accessory minerals. In photomicrographs, specks of fayalite interlocked within the abundant coarse-grained K-feldspars and amphibole crystals are discernable (Fig. 2i, j). Some fayalite crystals have been altered and partly replaced by pseudomorphs of Fe—Ti oxide (Fig. 2i). The clinopyroxene crystals commonly show zone textures with light pale cores and bright green rims (Fig. 2j).

The Dutse arfvedsonite aegirine granite are greyish coloured with coarse-grained or porphyritic textures. The essential minerals are perthite (45 vol%), quartz (20–25 vol%), aegirine (15 vol%) and arfvedsonite (10–15 vol%) with quartz grains occupying the junctions between the arfvedsonite and aegirine (Fig. 2k).

Porphyritic varieties of the Dutse arfvedsonite aegirine granite are coarse-grained in the groundmass. The rocks are light grey in colour, containing ~40–50 vol% phenocrysts (mostly 1–5 mm in size) that are mainly composed of quartz (10–15 vol%), K-feldspar (25–30 vol%) and euhedral plagioclase (5–10 vol%). The porphyritic texture is distinct at microscopic scale where large megacrysts of K-feldspar have rims of quartz or quartzofeldspathic fine intergrowths. The groundmass of the porphyritic arfvedsonite aegirine granite (Fig. 2l) comprises of quartz, arfvedsonite, aegirine and perthite with accessory zircon and apatite.

## 3. Analytical method

### 3.1. Mineral composition

Representative mineral (amphibole, pyroxene and biotite) compositions were determined by means of electron microprobe analysis (EMPA) using a JEOL JXA-8230 Superprobe at the Sample Solution An-

alytical Technology Co., Ltd. (Wuhan). Back-scattered electron (BSE) images of the representative minerals were taken with a scanning electron microscope coupled with an energy dispersive spectroscopy (EDS) system at the Sample Solution Analytical Technology Co., Ltd. (Wuhan). Quantitative analysis was carried out using a beam diameter of 3  $\mu\text{m}$ , an accelerating voltage of 15 kV and a beam current of 10 nA. Analytical precision is better than 1 wt% for major elements (contents >5 wt%). Raw data corrections for the atomic number and absorption effects were done with a ZAF program. The standard materials used are  $\text{Fe}_3\text{Al}_2\text{Si}_3\text{O}_{12}$  (Al, Si),  $\text{TiO}_2$  (Ti),  $\text{Fe}_2\text{O}_3$  (Fe),  $\text{MnSiO}_3$  (Mn),  $(\text{Mg}, \text{Fe})_2\text{SiO}_4$  (Mg),  $\text{CaSO}_4$  (Ca),  $\text{NaAlSi}_3\text{O}_8$  (Na),  $\text{KAlSi}_3\text{O}_8$  (K),  $\text{SrSO}_4$  (Sr), and  $\text{BaSO}_4$  (Ba). Mineral formulas and compositions in atoms per formula unit (apfu) were calculated from EPMA data based on 23 oxygen atoms for amphibole (after Li et al., 2020b), 22 oxygen atoms for biotite (after Yang and Lentz, 2005) and 4 cations and 6 oxygen atoms for pyroxene (after Morimoto, 1988).

### 3.2. Whole-rock major and trace element analysis

Representative samples were picked from the Daura and Dutse complex for geochemical analysis. For major and trace element analysis, five samples were selected from the Daura complex, and three samples were selected from the Dutse complex. The fresh samples were firstly cleaned by deionized water and crushed to powder using an agate mill. Major elements were ascertained at the Australian laboratory services (ALS) where an X-Ray fluorescence (ME-XRF26d) spectrometry method was used with analytical uncertainty of <5%, and detection limits of <0.01%. To measure trace and rare element compositions, fresh rock powders were digested using  $\text{HF} + \text{HNO}_3$  in Teflon bombs and later analyzed with an Agilent 7500a ICP-MS in the State Key Laboratory of Geological Process and Mineral Resources (GPMR) at China University of Geosciences (Wuhan). During each cylinder run, a background acquisition time of 20 – 30 s for gas blank and 50 s for data acquisition from the sampled were used. Sample digestion procedure employed for ICP-MS analyses has been described in detail by Liu et al. (2008).

### 3.3. Zircon U—Pb LA-ICPMS analysis

Two representative zircon samples from the Daura complex (amphibole syenite DA2-1 and biotite granite DA3-1) and three zircon samples from the Dutse (porphyritic arfvedsonite aegirine granite DT4-1, arfvedsonite aegirine granite DT4-2 and fayalite syenite DT2-2) were handpicked for U—Pb dating. The analysis was performed at Sample Solution Analytical Technology, Co. Ltd., Wuhan, China using a 193 nm GeolasPro Laser Ablation System and 170 Agilent 7700e ICP-MS instrument with a laser spot of 25  $\mu\text{m}$  corresponding to a frequency of 10 Hz. Zircon trace element and U—Pb dating performed using two (zircon 91,500 and GJ-1) reference materials as standards with background acquisition of about 20 to 30 s. Quantitative standardization of trace element and U—Pb isotopic data of zircons was performed using Excel-based ICPMS Data Cal software, according to procedures outlined by Liu et al. (2008). The excel-based program Isoplot v4.15 was used to generate weighted mean average and geochron Concordia diagrams. The results of the analyzed standards are given in Supplementary Table S1. Overall, the analyses yielded mean  $^{206}\text{Pb}/^{238}\text{U}$  ages of

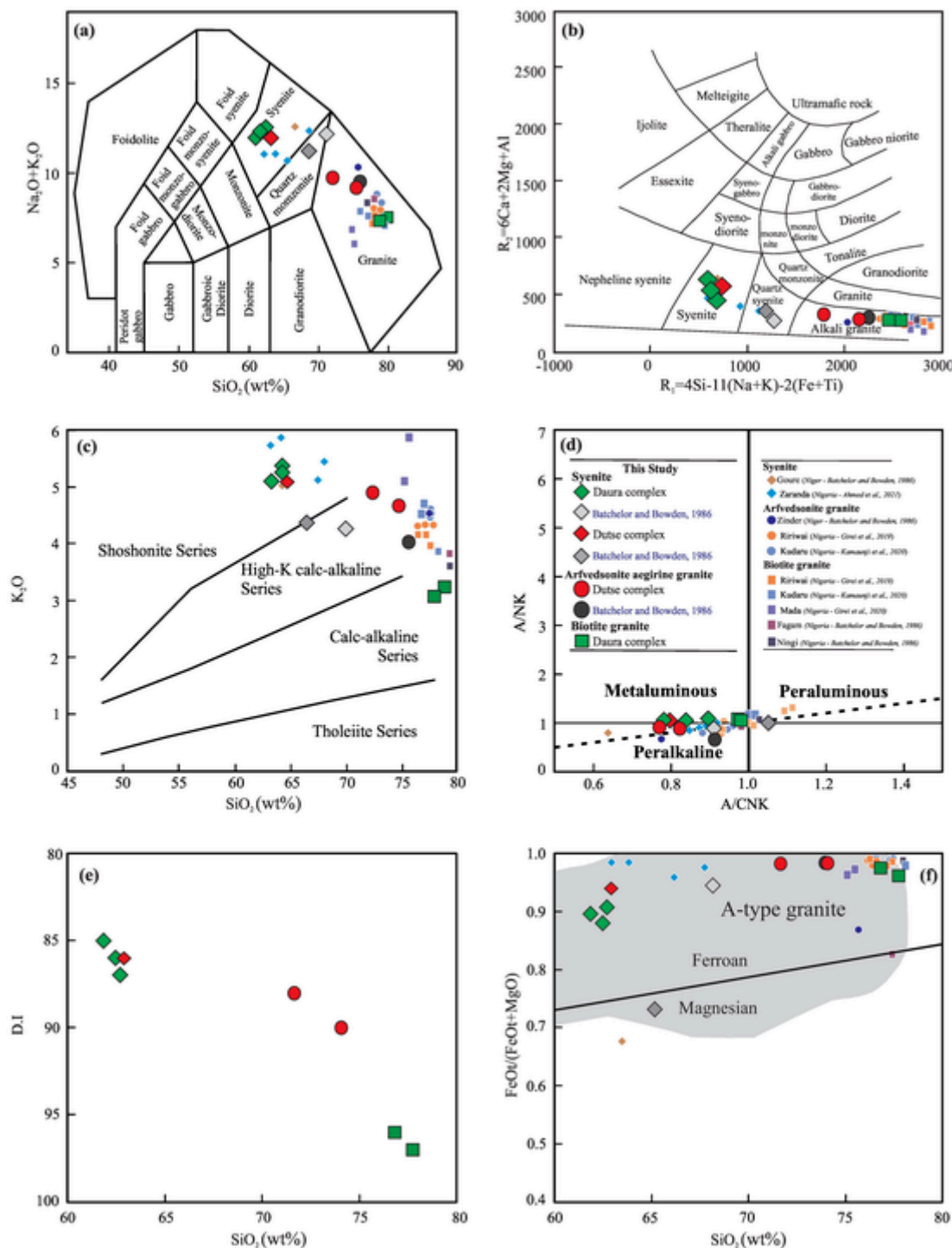


**Fig. 6.** (a) Chemical classification and nomenclature of Daura-Dutse granites using the total alkali versus silica (TAS) diagram (after Middlemost, 1994), (b) R1-R2 classification of the Daura-Dutse granites (after De la Roche et al., 1980), (c)  $\text{SiO}_2$  vs  $\text{K}_2\text{O}$ , (d) A/CNK versus A/NK diagram, (e) Differentiation index shown by DI ( $\text{Qz} + \text{Or} + \text{Ab} + \text{Ne} + \text{Lc} + \text{Ks}$ ) by normative percent; Thornton and Tuttle, 1960) vs.  $\text{SiO}_2$  plot, and (f)  $\text{FeOt}/(\text{MgO} + \text{FeOt})$  vs.  $\text{SiO}_2$  discrimination diagram for A-type granites. Data for comparison taken for the Goure (Niger Rep.), Zinder (Niger Rep.), Ningi, Zaranda and Fagam complexes are from Batchelor and Bowden (1986).

$569.9 \pm 2.1$  Ma (MSWD = 3.7,  $n = 6$ ) for GJ-1 and  $1062.7 \pm 3.0$  Ma (MSWD = 0.02,  $n = 13$ ) for 91,500 (Supplementary Fig. 1; Supplementary Table S1), which are consistent with recommended values within error limits (Jackson et al., 2004; Wiedenbeck et al., 2004).

#### 3.4. In-situ zircon Lu—Hf isotope analysis

In-situ zircon Lu—Hf isotopes were analyzed based on standard procedures for MC-ICP-MS and laser ablation system as put forth by Lizuka and Hirata. (2005). The analysis was carried out by use of a Neptune plus MC-ICP-MS with a combination of a Geolas 2005 excimer ArF laser ablation system at the GPMR. The calculation for  $\epsilon\text{Hf}(t)$  values

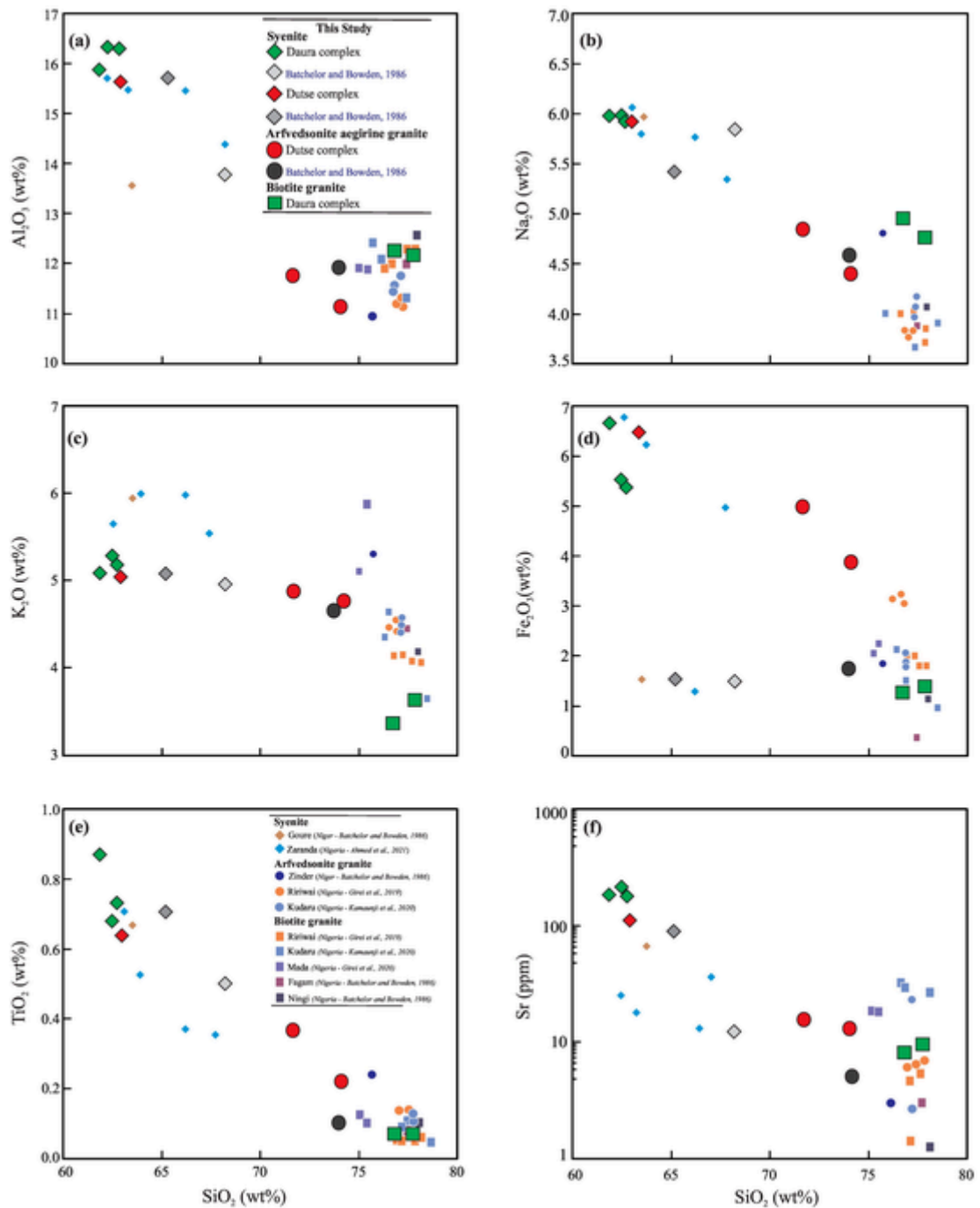


**Fig. 7.** Harker variation plots of  $\text{SiO}_2$  vs. (a)  $\text{Al}_2\text{O}_3$ , (b)  $\text{Na}_2\text{O}$ , (c)  $\text{K}_2\text{O}$ , (d)  $\text{TFe}_2\text{O}_3$ , (e)  $\text{TiO}_2$ , and (f)  $\text{Sr}$ . Data of granites plotted for comparisons are from Batchelor and Bowden (1986), Girei et al. (2019, 2020) and Kamaunji et al. (2020).

was made using present-day chondrite values of  $^{176}\text{Hf}/^{177}\text{Hf} = 0.2827$  and  $^{176}\text{Lu}/^{177}\text{Hf} = 0.0332$ . Zircon standard 91,500 yielded a weighted average  $^{176}\text{Hf}/^{177}\text{Hf}$  ratio of  $0.282308 \pm 0.000013$  ( $1\sigma$ ,  $n = 16$ ), GJ-1 and TEM yielded weighted average  $^{176}\text{Hf}/^{177}\text{Hf}$  ratios of  $0.282017 \pm 0.000011$  ( $1\sigma$ ,  $n = 6$ ) and  $0.282695 \pm 0.000011$  ( $1\sigma$ ,  $n = 6$ ), respectively. Single-stage depleted mantle model ages (TDM) was calculated based on present-day chondrite values of  $^{176}\text{Hf}/^{177}\text{Hf} = 0.28325$  and  $^{176}\text{Lu}/^{177}\text{Hf} = 0.0384$ . Two-stage model ages (T<sub>2DM</sub>) were calculated using the  $^{176}\text{Hf}/^{177}\text{Hf}$  ratio of 0.0150 for the average continental crust (Iizuka and Hirata, 2005).

### 3.5. Whole-rock Nd - Pb isotopic analysis

Four representative samples from both complexes were selected for bulk Sm-Nd/Pb-Pb isotope analysis performed at Sample Solution Analytical Technology, Co., Ltd., Wuhan, China, using the Neptune Plus MC-ICP-MS. Powdered samples were mixed with 1 ml HF and  $\text{HNO}_3$  in a stainless-Teflon bomb and dried in an electric oven for 24 h at 185 °C. Separation of Nd from other REE elements was achieved by repeat two-stage dissolution in 1 ml of  $\text{HNO}_3$  and 1 ml of 1 M HBr and subsequent drying. The Pb fraction was eluted using 1 M HCl and gently evaporated to dryness before mass-spectrometric measurement. Further standardization for values of  $^{208}\text{Pb}/^{204}\text{Pb} = 36.7262 \pm 31$ ,  $^{207}\text{Pb}/^{204}\text{Pb} = 15.5000 \pm 13$ ,  $^{206}\text{Pb}/^{204}\text{Pb} = 16.9416 \pm 13$  is based

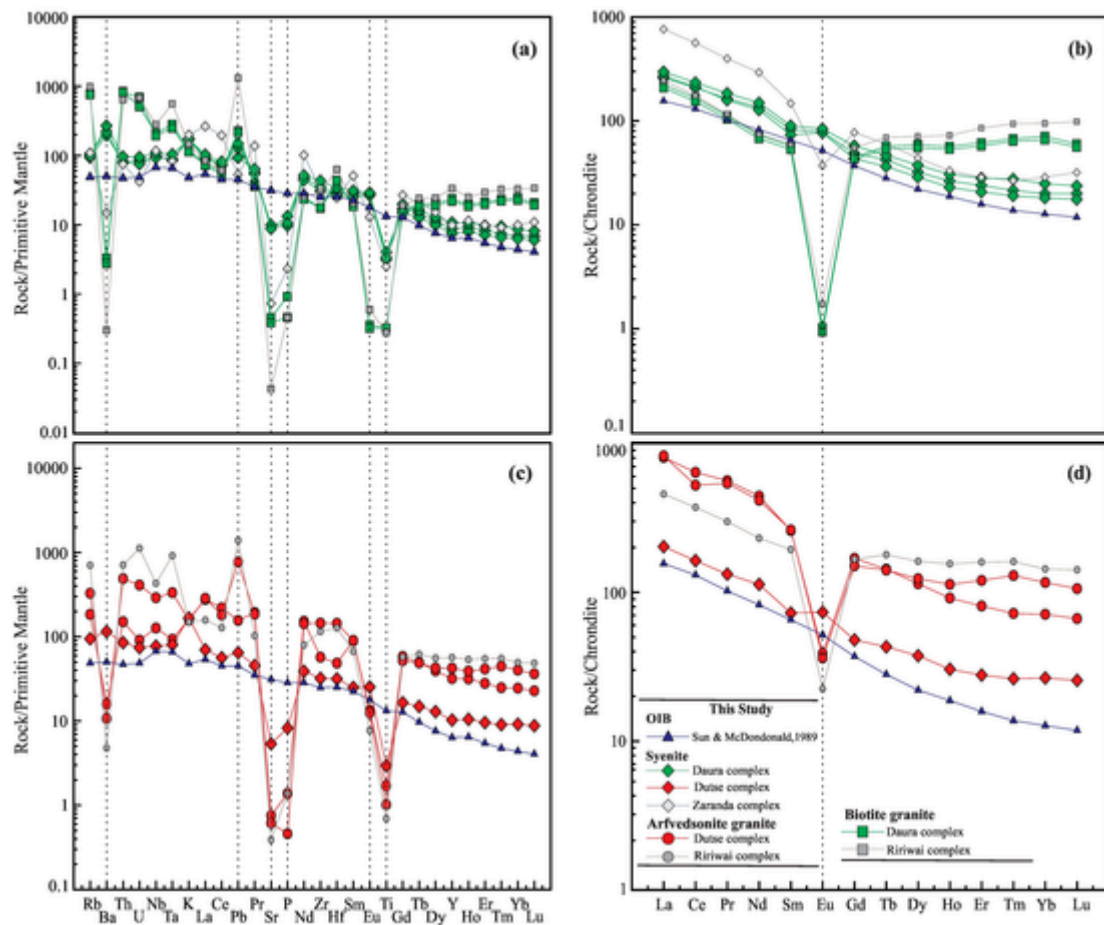


**Fig. 8.** Primitive mantle-normalized trace element spider diagrams of (a) Daura complex, (c) Dutse complex. Chondrite normalized rare earth element (REE) diagrams of (b) Daura complex, (d) Dutse complex. Data for comparison taken for Ririwai complexes and Ocean Island Basalts are from Bowden, (1985), Girei et al., (2019) and Sun and McDonough (1989). Normalization values used were taken from Sun and McDonough (1989) and Taylor and McLennan (1985), respectively.

on standard NBS SRM 981. The  $^{143}\text{Nd}/^{144}\text{Nd}$  ratio of  $0.512118 \pm 15$  ( $2\sigma$ ,  $n = 31$ ) with an error limit of  $0.512115 \pm 07$  was also incorporated for data standardization purposes.

Detailed analytical procedures and sample preparation are described in Wang et al. (2018a).

## 4. Results

### 4.1. Mineral chemistry

#### 4.1.1. Amphibole

The amphibole compositions from the Daura amphibole syenite, Dutse fayalite syenite and Dutse arfvedsonite aegirine granite are given in Supplementary Table S2. On the BSE images, amphiboles from the Daura syenite show zonation textures with light and grey bands along grain rim and core (Fig. 3a). Amphibole grains from the Dutse arfvedsonite aegirine granite commonly coexist with aegirine (Fig. 3b). On the chemical discrimination plot (after Hawthorne et al., 2012), the amphiboles from the Daura and Dutse syenite show a range of compositions from barrosite to winchite (Fig. 3c; after Hawthorne et al., 2012). In comparison, the amphiboles from the Daura arfvedsonite aegirine granite plot mostly as arfvedsonite (Fig. 3c). Plot of  $\text{Fe}^{2+}/(\text{Fe}^{2+} + \text{Mg}^{2+})$  vs.  $\text{Al}^{\text{VI}}$  show that the amphibole grains from the Dutse syenite and Dutse arfvedsonite aegirine granite and the amphibole rims of the Daura syenite largely formed under low oxygen fugacity conditions (Fig. 3d), typical of amphiboles found in A-type granites (Papoutsas and Pe-Piper, 2014). On the other hand, the amphibole cores of the Daura amphibole syenite show intermediate oxygen fugacity

conditions likely reflecting amphibole crystallization from melts enriched in magnesium (Papoutsas and Pe-Piper, 2014). Compared to core zones, amphibole rim compositions from the Daura syenite show a marked decrease in peralkalinity and a decrease in Fox oxidation ratios (Fig. 3e). Higher contents of Na and Si and lower contents of Ca and Al are apparent in the amphiboles from the Daura arfvedsonite aegirine granite than those from the Daura and Dutse syenite (Fig. 3f-h).

#### 4.1.2. Biotite

Subhedral biotite grains from the Daura amphibole syenite and biotite granite (Fig. 4a) were chosen for analysis and their compositions are shown in Supplementary Table S3. Biotite from the Daura amphibole syenite shows lower  $\text{FeO}_{\text{Total}}$  (34.9–36.0 wt%) and higher  $\text{MgO}$  (2.19–2.94 wt%) contents than those from the Daura biotite granite ( $\text{FeO}_{\text{Total}} = 37.20$ –40.52 wt%;  $\text{MgO} = 0.44$ –0.51 wt%). In the ternary diagram of  $\text{Mg}(\text{Al} + \text{Fe}^{3+} + \text{Ti})(\text{Fe}^{2+} + \text{Mn})$  (Fig. 4b; after Foster, 1960), biotite grains from the Daura syenite plot in the field of siderophyllites, whilst those from the Daura biotite granite straddle the boundary between ferri-muscovite and siderophyllite. In the ternary diagram of  $\text{MgO}-\text{FeO}-\text{Al}_2\text{O}_3$  (Fig. 4c), the biotite grains from both the Daura syenite and Daura biotite granite plot in the field of anorogenic alkaline to peraluminous suites. Biotite grains from the Daura amphibole syenite are poor in F (0.02–0.10 wt%),  $\text{Na}_2\text{O}$  (0.03–0.14 wt%), and  $\text{TiO}_2$  (0.68–1.12 wt%) as compared to those from Daura biotite granite ( $\text{F} = 2.94$ –3.79 wt%;  $\text{Na}_2\text{O} = 0.20$ –0.32 wt%;  $\text{TiO}_2 = 1.59$ –2.25 wt%).

**Table 2**

LA-ICP-MS Zircon U—Pb data for the Daura and Dutse complexes.

Analysis	Element Conc.		Element Ratios	Isotopic Ratios						Isotopic Ages (Ma)						
	Th	U		$^{207}\text{Pb}/^{206}\text{Pb}$	1 $\sigma$	$^{207}\text{Pb}/^{235}\text{U}$	1 $\sigma$	$^{206}\text{Pb}/^{238}\text{U}$	1 $\sigma$	$^{207}\text{Pb}/^{206}\text{Pb}$	1 $\sigma$	$^{207}\text{Pb}/^{235}\text{U}$	1 $\sigma$	$^{206}\text{Pb}/^{238}\text{U}$	1 $\sigma$	Conc.
<b>Daura amphibole syenite (DA2-1)</b>																
DA2-2-1	82	323	0.83	0.0501	0.0021	0.3627	0.0154	0.0519	0.0006	211	96	314	11	326	3	96%
DA2-2-2	1643	7309	2.40	0.0503	0.0012	0.3587	0.0082	0.0513	0.0005	209	54	311	6	323	3	96%
DA2-2-3	116	444	0.78	0.0535	0.0018	0.3832	0.0129	0.0515	0.0005	350	50	329	9	324	3	98%
DA2-2-5	180	729	0.87	0.0514	0.0016	0.3662	0.0110	0.0514	0.0004	261	70	317	8	323	3	98%
DA2-2-6	254	1017	0.98	0.0526	0.0019	0.3803	0.0128	0.0522	0.0005	309	81	327	9	328	3	99%
DA2-2-7	773	3305	1.67	0.0516	0.0013	0.3696	0.0093	0.0516	0.0005	265	59	319	7	324	3	98%
DA2-2-8	177	725	0.91	0.0520	0.0016	0.3681	0.0109	0.0511	0.0004	283	68	318	8	321	3	99%
DA2-2-9	177	735	1.00	0.0521	0.0017	0.3692	0.0119	0.0509	0.0004	300	74	319	9	320	3	99%
DA2-2-10	456	1912	1.30	0.0528	0.0015	0.3820	0.0106	0.0522	0.0005	320	65	329	8	328	3	99%
DA2-2-11	1450	6562	3.37	0.0521	0.0014	0.3752	0.0097	0.0519	0.0005	300	61	323	7	326	3	99%
DA2-2-12	313	1313	1.24	0.0503	0.0014	0.3605	0.0104	0.0515	0.0004	209	67	313	8	324	3	96%
DA2-2-13	1856	8217	2.55	0.0503	0.0012	0.3652	0.0088	0.0523	0.0005	209	577	316	6	329	3	96%
DA2-2-14	107	437	0.93	0.0516	0.0019	0.3703	0.0132	0.0517	0.0005	333	83	320	10	325	3	98%
DA2-2-15	180	739	1.11	0.0525	0.0017	0.3775	0.0116	0.0520	0.0005	306	72	325	8	327	3	99%
DA2-2-16	311	1331	1.22	0.0520	0.0014	0.3728	0.0101	0.0516	0.0004	287	58	322	7	324	2	99%
DA2-2-17	145	556	0.96	0.0576	0.0021	0.4182	0.0154	0.0521	0.0005	517	78	355	11	328	3	92%
DA2-2-18	189	782	0.97	0.0519	0.0015	0.3675	0.0104	0.0510	0.0004	280	65	318	8	321	3	99%
DA2-2-19	427	1809	1.51	0.0521	0.0014	0.3767	0.0100	0.0522	0.0005	287	56	325	7	328	3	99%
<b>Daura biotite granite (DA3-1)</b>																
DA3-2	320	353	1.05	0.0559	0.0056	0.4001	0.0358	0.0513	0.0014	456	222	342	25	322	8	94%
DA3-14	249	397	0.63	0.0528	0.0022	0.3661	0.0142	0.0512	0.0009	320	89	317	10	322	5	98%
DA3-16	229	383	0.60	0.0539	0.0023	0.3824	0.0164	0.0513	0.0009	369	63	329	12	322	5	97%
DA3-20	223	465	0.48	0.0603	0.0038	0.4109	0.0246	0.0517	0.0020	617	135	350	17	325	12	92%
DA3-1	217	371	0.58	0.0784	0.0069	0.5538	0.0462	0.0516	0.0018	1167	174	447	30	324	11	68%
DA3-9	912	460	1.98	0.1050	0.0048	0.7045	0.0296	0.0513	0.0018	1714	84	541	17	322	11	49%
DA3-17	640	857	0.75	0.0916	0.0031	0.6449	0.0224	0.0509	0.0010	1458	65	505	14	320	6	55%
DA3-13	875	493	1.77	0.0880	0.0061	0.5602	0.0502	0.0471	0.0025	1383	132	452	33	297	15	58%
DA3-3	32,304	9596	3.36	0.2031	0.0053	0.3057	0.0100	0.0110	0.0003	2851	42	271	7	70.4	2	-18%
DA3-4	73,540	18,631	3.94	0.2442	0.0055	0.4218	0.0096	0.0125	0.0002	3148	35	357	6	80.3	1	-27%
DA3-5	11,249	6221	1.81	0.2717	0.0067	0.27145	0.0868	0.0726	0.0019	3316	39	1332	24	452	11	1%
DA3-7	13,088	3193	4.09	0.2006	0.0068	0.7692	0.0362	0.0273	0.0008	2831	56	579	20	174	5	-8%
DA3-8	14,750	21,833	0.67	0.2578	0.0072	0.7004	0.0307	0.0199	0.0008	3235	44	539	18	127	5	-24%
DA3-10	2666	3049	0.87	0.1897	0.0063	0.9150	0.0284	0.0358	0.0009	2739	55	660	15	227	6	2%
DA3-11	33,594	14,942	2.24	0.2523	0.0054	0.8095	0.0182	0.0232	0.0003	3199	34	602	10	148	2	-22%
DA3-12	13,982	2375	5.88	0.2293	0.0060	0.23902	0.0655	0.0757	0.0015	3047	41	1240	20	470	9	10%
DA3-15	31,629	8196	3.85	0.2389	0.0055	1.3164	0.0306	0.0398	0.0006	3113	37	853	13	251	4	-9%
DA3-19	1959	3021	0.64	0.1335	0.0050	0.3814	0.0279	0.0206	0.0012	2146	65	328	21	131	7	14%
<b>Dutse fayalite syenite (DT2-2)</b>																
DT2-2-1	579	654	0.88	0.0505	0.0019	0.2557	0.0095	0.0365	0.0004	220	89	231	8	231	2	99%
DT2-2-2	385	469	0.82	0.0499	0.0021	0.2546	0.0105	0.0367	0.0004	191	100	230	8	232	2	99%
DT2-2-3	686	689	0.99	0.0539	0.0024	0.2754	0.0121	0.0368	0.0004	365	98	247	10	233	2	94%
DT2-2-4	844	791	1.06	0.0501	0.0017	0.2545	0.0081	0.0366	0.0003	198	76	230	6	232	2	99%
DT2-2-5	368	463	0.79	0.0511	0.0025	0.2594	0.0120	0.0367	0.0004	256	111	234	10	232	2	99%
DT2-2-6	580	624	0.93	0.0495	0.0019	0.2527	0.0096	0.0368	0.0003	172	91	229	8	233	2	98%
DT2-2-7	537	610	0.88	0.0511	0.0021	0.2589	0.0106	0.0366	0.0004	256	96	234	8	232	2	99%
DT2-2-9	810	744	1.08	0.0514	0.0023	0.2627	0.0112	0.0369	0.0004	257	106	237	9	233	3	98%
DT2-2-10	1480	1262	1.17	0.0508	0.0016	0.2593	0.0081	0.0367	0.0004	232	69	234	6	232	2	99%
DT2-2-11	659	686	0.96	0.0511	0.0019	0.2601	0.0094	0.0367	0.0004	243	80	235	7	233	2	99%
DT2-2-12	1776	1241	1.43	0.0499	0.0015	0.2540	0.0074	0.0367	0.0003	187	70	230	6	232	2	99%
DT2-2-13	686	736	0.93	0.0509	0.0020	0.2609	0.0099	0.0368	0.0004	239	89	235	8	233	2	99%
DT2-2-14	730	731	0.99	0.0506	0.0035	0.2578	0.0175	0.0367	0.0004	220	159	233	14	232	2	99%
DT2-2-15	559	604	0.92	0.0506	0.0022	0.2587	0.0112	0.0367	0.0004	233	100	234	9	232	2	99%
DT2-2-16	509	552	0.92	0.0508	0.0024	0.2574	0.0121	0.0366	0.0005	232	109	233	10	232	3	99%
<b>Dutse porphyritic arfvedsonite aegirine syenite (DT4-1)</b>																
DT4-1-1	312	415	0.75	0.0524	0.0032	0.2954	0.0185	0.0412	0.001	306	134	263	14	260	6	99%
DT4-1-2	31.3	61.1	0.51	0.0754	0.0535	0.2896	0.0964	0.041	0.0018	1080	1004	258	76	259	11	99%
DT4-1-5	44.9	61.6	0.72	0.0461	0.0435	0.3015	0.0921	0.0428	0.0016	400	1016	268	72	270	10	99%
DT4-1-6	44.4	72.2	0.56	0.0664	0.0118	0.2929	0.0562	0.0416	0.0014	817	380	261	44	263	9	99%
DT4-1-7	28.9	59.3	0.49	0.0572	0.0205	0.2908	0.1000	0.0411	0.0020	502	637	259	79	260	13	99%
DT4-1-8	43.8	74.4	0.59	0.0626	0.0103	0.3181	0.0518	0.0417	0.0015	694	355	280	40	264	9	93%

(continued on next page)

Table 2 (continued)

Analysis	Element Conc. (ppm)		Element Ratios	Isotopic Ratios								Isotopic Ages (Ma)							
	Th	U		$^{207}\text{Pb}/^{206}\text{Pb}$	1 $\sigma$	$^{207}\text{Pb}/^{235}\text{U}$	1 $\sigma$	$^{206}\text{Pb}/^{238}\text{U}$	1 $\sigma$	$^{207}\text{Pb}/^{206}\text{Pb}$	1 $\sigma$	$^{207}\text{Pb}/^{235}\text{U}$	1 $\sigma$	$^{206}\text{Pb}/^{238}\text{U}$	1 $\sigma$	Conc.			
DT4-1-9	24.1	73.8	0.33	0.0493	0.0090	0.2904	0.0521	0.0410	0.0017	167	372	259	41	259	11	99%			
DT4-1-10	34.6	63.5	0.54	0.0508	0.0111	0.2924	0.0632	0.0415	0.0020	232	440	260	50	262	12	99%			
DT4-1-11	24.3	49.1	0.49	0.0626	0.0161	0.2927	0.0648	0.0414	0.0018	694	565	261	50	261	11	99%			
DT4-1-12	44.4	72.2	0.31	0.0664	0.0118	0.2929	0.0562	0.0416	0.0014	817	380	261	44	263	8	99%			
DT4-1-13	24.2	57.9	0.61	0.0847	0.0262	0.2993	0.0627	0.0417	0.0025	1309	632	266	49	264	15	99%			
DT4- 1 – 14	32.2	67	0.42	0.0476	0.0138	0.3040	0.1293	0.0410	0.0019	76	577	270	100	259	12	99%			
DT4-1-15	28.7	51.3	0.48	0.0612	0.0199	0.3379	0.1146	0.0473	0.0020	656	577	296	87	298	12	96%			
Dutse arfvedsonite aegirine granite (DT4-2)																			
DT4-2-3	59.3	81.2	0.73	0.0529	0.0080	0.2354	0.0344	0.0340	0.0007	324	311	215	28	215	4	99%			
DT4-2-7	794	360	2.20	0.0575	0.0036	0.2920	0.0178	0.0369	0.0004	522	137	260	13	233	2	90%			
DT4-2-10	43.1	78.4	0.55	0.0505	0.0057	0.2616	0.0305	0.0375	0.0007	217	244	236	24	237	4	99%			
DT4-2-12	16.1	46.6	0.34	0.0589	0.0157	0.2620	0.0714	0.0371	0.0016	561	497	236	57	235	10	99%			
DT4-2-13	47.7	75.7	0.63	0.0567	0.0072	0.2603	0.0332	0.0370	0.0008	480	284	235	26	234	4	99%			
DT4-2-14	132	91.9	1.44	0.0528	0.0056	0.2604	0.0259	0.0369	0.0006	320	242	235	20	234	3	99%			
DT4-2-15	45.0	70.4	0.64	0.0516	0.0056	0.2672	0.0284	0.0380	0.0009	333	164	240	22	240	5	99%			
DT4-2-16	89.4	114	0.79	0.0502	0.0053	0.2559	0.0273	0.0363	0.0006	206	229	231	22	230	3	99%			
DT4-2-2	46.3	75.7	0.61	0.0749	0.0081	0.3603	0.0369	0.0352	0.0008	1133	220	312	28	223	5	66%			
DT4-2-1	150	227	0.66	0.7714	0.0198	25.3737	0.6511	0.2360	0.0028	error	error	3322	25	1365	14	16%			
DT4-2-4	1283	239	5.36	0.1664	0.0063	0.9778	0.0378	0.0424	0.0006	2521	63	692	19	267	4	11%			
DT4-2-5	323	288	1.21	0.3590	0.0085	2.9555	0.0715	0.0594	0.0007	3745	36	1396	18	371	4	-16%			
DT4-2-6	1230	410	3.00	0.1908	0.0059	1.1884	0.0369	0.0449	0.0005	2750	50	795	17	283	3	4%			
DT4-2-8	299	199	1.50	0.5813	0.0132	8.2152	0.1741	0.1019	0.0010	4462	33	2255	19	625	6	-14%			
DT4-2-9	588	217	2.71	0.4869	0.0113	5.2764	0.1157	0.0783	0.0008	4202	34	1865	18	486	5	-18%			
DT4-2-11	91.8	63.6	1.44	0.6263	0.0180	11.2969	0.3569	0.1311	0.0026	4570	41	2548	29	794	15	-5%			

#### 4.1.3. Pyroxene

The composition of analyzed clinopyroxenes (Cpx) from the Daura amphibole syenite, Dutse fayalite syenite and Dutse arfvedsonite aegirine granite are presented in Supplementary Table S4. The Cpx crystals from the Daura syenite compositionally plot in the hedenbergite field in the  $\text{Al}^{\text{VI}}/(\text{Al}^{\text{VI}} + \text{Fe}^{3+})$  vs.  $\text{Na}/(\text{Na} + \text{Ca})$  discrimination plot (Fig. 5a), while those from the Dutse fayalite syenite trend from herdenbergite to aegirine-augite (Fig. 5a). The Cpx crystals from the Daura arfvedsonite aegirine granite mostly show aegirine compositions (Fig. 5a). On the Aeg-Di-Hed triangle diagram (Fig. 5b; after Coulson, 2003), the Cpx chemically evolve from diopside-hedenbergite of the Daura amphibole syenite, through the hedenbergite of the Dutse fayalite syenite to the aegirine of the Dutse arfvedsonite aegirine granite, similar to the evolution trends observed in North Qurog alkaline complex, South Greenland (trend 6; Fig. 5b). All analyzed Cpx data points show a marked negative correlation between  $\text{Ca} + \text{Mg} + \text{Fe}^{2+}$  and  $\text{Na} + \text{Fe}^{3+}$  (Fig. 5c), consistent with the substitution mechanism of  $(\text{Mg}/\text{Fe})^{2+} + \text{Ca}^{2+} \leftrightarrow \text{Fe}^{3+} + \text{Na}^+$ . A compositional profile has been conducted on the zoned clinopyroxene from the Dutse fayalite syenite (Fig. 5d). From core to rim, a notable increase in  $\text{Na}$ ,  $\text{Fe}^{3+}$  and Fox values (Fig. 5e–g) and a corresponding drop in  $\text{Al}$ ,  $\text{Ca}$ ,  $\text{Fe}^{2+}$ ,  $\text{Ti}$  and  $\text{Mg}$  values are present (Fig. 5h–l).

#### 4.2. Whole-rock major and trace element compositions

##### 4.2.1. Whole-rock major elements

Whole-rock major element compositions of the Daura and Dutse samples are given in Table 1. In the total alkali vs silica (TAS) and R1-R2 diagrams after Middlemost (1994) and De la Roche et al. (1980), the studied samples plot in fields consistent with petrographic observations (Fig. 6a, b). The Daura and Dutse syenites have moderate  $\text{SiO}_2$  contents of 61.84 to 62.90 wt% (mean of 62.49 wt%) which are lower than the Daura arfvedsonite aegirine granite ( $\text{SiO}_2 = 71.65\text{--}74.05$  wt%, mean of 72.85 wt%) and Daura biotite granite ( $\text{SiO}_2 = 76.81\text{--}77.75$  wt%, mean of 77.28 wt%; Table 1). The  $\text{Al}_2\text{O}_3$  (15.64–16.31 wt%),  $\text{Fe}_2\text{O}_3$  (5.36–6.66 wt%),  $\text{K}_2\text{O}$  (5.04–5.28 wt%),  $\text{TiO}_2$  (0.64–0.87 wt%) and  $\text{P}_2\text{O}_5$  (0.18–0.29 wt%) contents of the Daura and Dutse syenites are

much higher than those of the Dutse arfvedsonite aegirine granite ( $\text{Al}_2\text{O}_3 = 11.16\text{--}11.78$  wt%,  $\text{Fe}_2\text{O}_3 = 3.88\text{--}5.01$  wt%;  $\text{K}_2\text{O} = 4.72\text{--}4.89$  wt%,  $\text{TiO}_2 = 0.22\text{--}0.37$  wt%;  $\text{P}_2\text{O}_5 = 0.01\text{--}0.03$  wt%) and Daura biotite granite ( $\text{Al}_2\text{O}_3 = 12.18\text{--}12.26$  wt%;  $\text{Fe}_2\text{O}_3 = 1.28\text{--}1.38$  wt%;  $\text{K}_2\text{O} = 3.39\text{--}3.61$  wt%;  $\text{TiO}_2 = 0.07\text{--}0.08$  wt%;  $\text{P}_2\text{O}_5 = 0.01\text{--}0.02$  wt%; Table 1). The Daura and Dutse syenites both plot in the shonshonitic field on the  $\text{SiO}_2$  vs  $\text{K}_2\text{O}$  diagram (Fig. 6c), while the Dutse arfvedsonite aegirine granite and Daura biotite granite plot as calc-alkaline to high K calc-alkaline granites. On the ANK vs ACNK diagram (Fig. 6d), the Daura and Dutse syenites and Daura biotite granite all plot on the boundary between metaluminous and peralkaline granite fields, whereas the Dutse arfvedsonite aegirine granite plot in the peralkaline granite field. The calculated alkalinity ratios ( $[\text{Al}_2\text{O}_3 + \text{CaO} + (\text{Na}_2\text{O} + \text{K}_2\text{O})]/[\text{Al}_2\text{O}_3 + \text{CaO} - (\text{Na}_2\text{O} + \text{K}_2\text{O})]$ ; after Wright, 1969) are lower in the Daura and Dutse syenites (4.19–4.44) and Daura biotite granite (4.88–5.10) than the arfvedsonite aegirine granite (8.41–8.78). The calculated differentiation indexes using normative mineral contents for the Daura-Dutse suites (D.I. =  $\text{Qz} + \text{Or} + \text{Ab} + \text{Ne} + \text{Lc} + \text{Ks}$ ; after Thornton and Tuttle, 1960) increase from the Daura and Dutse syenites (85–87), through the Dutse arfvedsonite aegirine granite (88–90) to the Daura biotite granite (96–97) (Fig. 6e; Table 1). All the studied syenites and granites show ferroan compositions and plot in the A-type granite field (Fig. 6f; after Frost and Frost, 2001). In the Harker diagrams (Fig. 7), the studied samples show decreasing trends of  $\text{Al}_2\text{O}_3$ ,  $\text{Na}_2\text{O}$ ,  $\text{K}_2\text{O}$ ,  $\text{Fe}_2\text{O}_3\text{Total}$ ,  $\text{TiO}_2$  and  $\text{Sr}$  with increasing  $\text{SiO}_2$ .

##### 4.2.2. Trace and rare earth element (REE)

The Daura amphibole syenite and Dutse fayalite syenite show similar trace element variations and patterns as well (Table 1). They have moderate  $\text{Sr}$  (113–210 ppm),  $\text{Nb}$  (55–78 ppm),  $\text{Zr}$  (346–484 ppm) and variable  $\text{Th}$  contents (6.72–8.14 ppm). In the primitive mantle-normalized trace element diagrams (Fig. 8a, c), the syenites show positive anomalies of  $\text{Ba}$  and  $\text{Pb}$  and negative anomalies of  $\text{Sr}$ ,  $\text{P}$  and  $\text{Ti}$ . Rare earth element (REE) patterns for the Daura amphibole syenite and Dutse fayalite syenite are characterized by slight enrichments of LREE

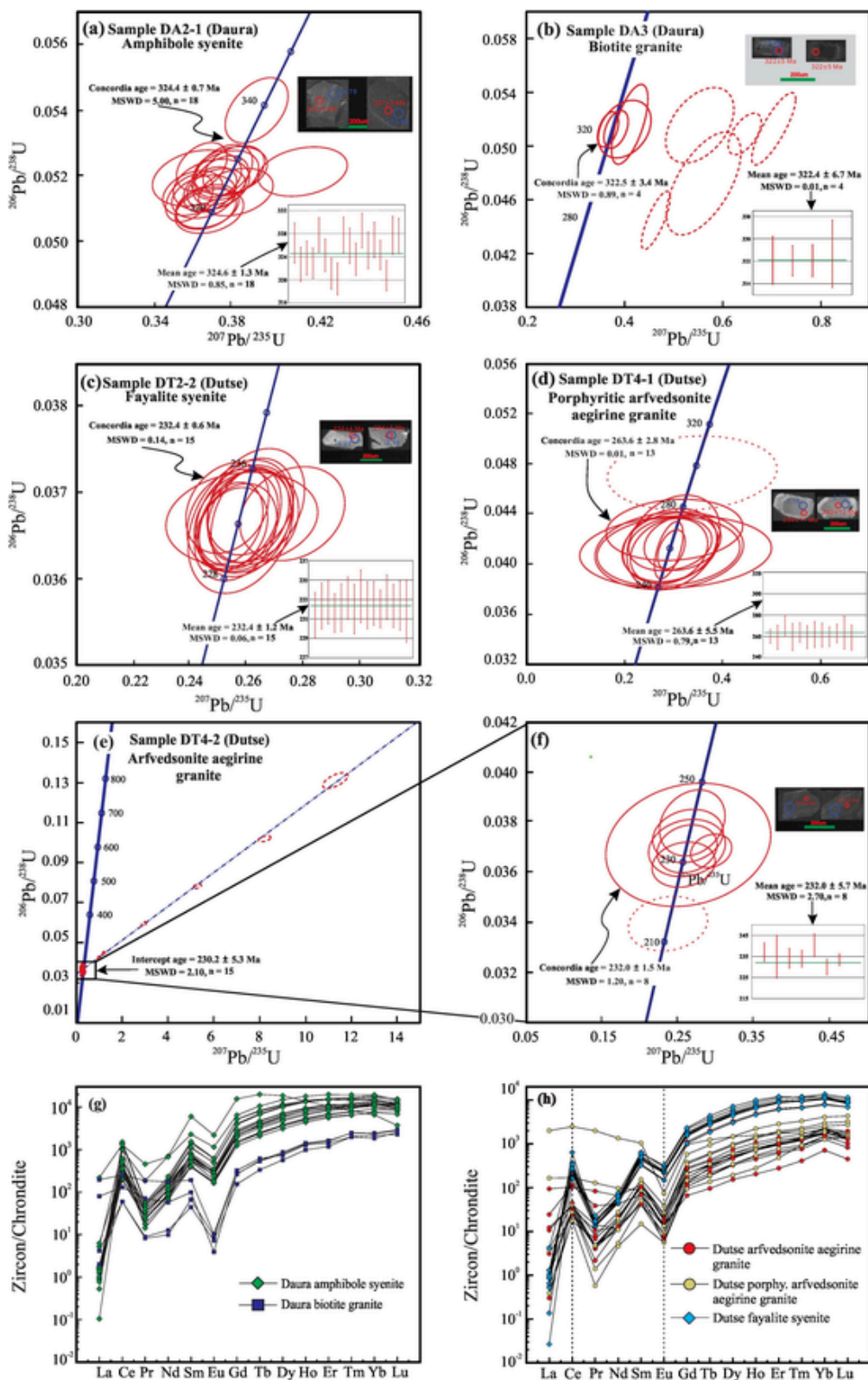


**Fig. 9.** a-d. LA-ICP-MS zircon U—Pb age concordia plots for (a) Daura amphibole syenite (DA2), (b) Daura biotite granite (DA3), (c) Dutse fayalite syenite (DT2), and (d) Dutse porphyritic arfvedsonite aegirine granite (DT4–1). (e) Intercept age plot for Dutse arfvedsonite aegirine granite (DT4–2), and (f) zoomed zircon U—Pb age concordia plot for Fig. 9e. Fig. 6g–h Chondrite-normalized Zircon REE plots for concordant zircon grains from the (g) Daura complex and (h) Dutse complex. Dashed ellipses represent discordant zircon grains likely as a result of Pb-loss. Red circles represent U—Pb dating spots, and blue circles indicate Lu—Hf isotope analytical spots. The scale bar is 200  $\mu\text{m}$ . Normalization values were taken from Nakamura (1974).

**Table 3**  
Zircon in-situ Lu—Hf isotopic compositions for Daura and Dutse rocks.

Spot No	$^{176}\text{Yb}/^{177}\text{Hf}$	$^{176}\text{Lu}/^{177}\text{Hf}$	$^{176}\text{Hf}/^{177}\text{Hf}$	$\pm 1\sigma$	$\epsilon\text{Hf(t)}$	TDM(Ma)	TDM2(Ma)	$f\text{Lu/Hf}$
<b>Sample DA2 (Daura amphibole syenite)</b>								
DA2-2-1	0.247001	0.004990	0.282820	0.00002	7.75	685	774	-0.85
DA2-2-3	0.326363	0.005257	0.282850	0.00003	8.75	643	719	-0.84
DA2-2-5	0.457736	0.008312	0.282933	0.00004	11.05	561	590	-0.75
DA2-2-6	0.429324	0.007074	0.283012	0.00002	14.12	405	418	-0.79
DA2-2-7	0.409943	0.007557	0.282909	0.00002	10.34	589	630	-0.77
DA2-2-8	0.462228	0.007563	0.282927	0.00009	10.99	558	593	-0.77
DA2-2-9	0.078639	0.000858	0.283033	0.00001	16.17	309	303	-0.97
DA2-2-11	0.443170	0.007366	0.283087	0.00002	16.70	280	273	-0.78
DA2-2-12	0.355181	0.006307	0.283025	0.00004	14.73	374	384	-0.81
DA2-2-13	0.430096	0.007825	0.283002	0.00002	13.60	432	447	-0.76
<b>Sample DA3 (Daura biotite granite)</b>								
DA3-1	0.038678	0.000786	0.282602	0.00001	0.89	915	1281	-0.98
DA3-2	0.040763	0.000867	0.28259	0.00001	0.45	934	1309	-0.97
DA3-3	0.073793	0.001592	0.28259	0.00001	0.30	952	1319	-0.95
DA3-6	0.074499	0.001539	0.282587	0.00001	0.20	955	1325	-0.95
DA3-7	0.041187	0.000866	0.28260	0.00001	0.80	920	1286	-0.97
DA3-8	0.073715	0.001481	0.282614	0.00002	1.17	915	1263	-0.96
DA3-9	0.032589	0.000702	0.282595	0.00001	0.66	923	1295	-0.98
<b>Sample DT2 (Dutse fayalite syenite)</b>								
DT2-1	0.219155	0.005609	0.282769	0.00002	4.12	781	903	-0.83
DT2-2	0.239965	0.006003	0.282778	0.00002	4.39	775	888	-0.82
DT2-3	0.161401	0.004028	0.282797	0.00001	5.35	702	835	-0.88
DT2-4	0.268035	0.006640	0.282808	0.00002	5.37	740	834	-0.8
DT2-5	0.139805	0.003541	0.282751	0.00002	3.82	761	920	-0.89
DT2-6	0.188455	0.004263	0.282767	0.00002	4.28	752	894	-0.87
DT2-7	0.208025	0.005012	0.282780	0.00002	4.62	748	875	-0.85
DT2-8	0.264063	0.006294	0.282809	0.00002	5.43	731	830	-0.81
DT2-9	0.203393	0.004094	0.282786	0.00002	4.95	720	857	-0.88
DT2-11	0.216470	0.004741	0.282755	0.00002	3.76	782	923	-0.86
DT2-12	0.212434	0.004382	0.282797	0.00001	5.31	708	837	-0.87
DT2-13	0.148657	0.003194	0.282794	0.00002	5.39	689	833	-0.9
<b>Sample DT4-1 (Dutse porphyritic arfvedsonite aegirine granite)</b>								
DT4-1-1	0.019271	0.000443	0.282547	0.00001	-2.27	984	1436	-0.99
DT4-1-2	0.087979	0.002313	0.282587	0.00001	-1.18	977	1367	-0.93
DT4-1-3	0.010880	0.000256	0.282524	0.00001	-3.06	1012	1486	-0.99
DT4-1-4	0.058449	0.001701	0.282539	0.00001	-2.75	1028	1467	-0.95
DT4-1-5	0.061234	0.001671	0.282562	0.00001	-1.95	995	1416	-0.95
DT4-1-6	0.030496	0.000883	0.282547	0.00001	-2.33	995	1440	-0.97
DT4-1-7	0.037293	0.001058	0.282537	0.00001	-2.72	1014	1464	-0.97
DT4-1-8	0.051892	0.001427	0.282578	0.00001	-1.34	966	1377	-0.96
DT4-1-9	0.010808	0.000254	0.282558	0.00001	-1.84	964	1409	-0.99
DT4-1-10	0.070304	0.001957	0.282556	0.00001	-2.19	1011	1431	-0.94
<b>Sample DT4-2 (Dutse arfvedsonite aegirine granite)</b>								
DT4-2-1	0.070719	0.001429	0.282573	0.00002	-2.16	973	1405	-0.96
DT4-2-2	0.054598	0.001135	0.282555	0.00001	-2.78	991	1444	-0.97
DT4-2-3	0.101201	0.002122	0.282585	0.00001	-1.84	974	1385	-0.94
DT4-2-4	0.056878	0.001237	0.282540	0.00001	-3.30	1015	1477	-0.96
DT4-2-5	0.031266	0.000465	0.282573	0.00001	-2.00	948	1395	-0.99
DT4-2-6	0.007493	0.000124	0.282537	0.00001	-3.23	989	1472	-1
DT4-2-7	0.107516	0.001751	0.282530	0.00002	-3.75	1044	1505	-0.95
DT4-2-8	0.029850	0.000506	0.282573	0.00001	-2.02	949	1396	-0.98
DT4-2-9	0.071988	0.001465	0.282572	0.00001	-2.19	975	1407	-0.96
DT4-2-10	0.028662	0.000448	0.282578	0.00001	-1.84	941	1385	-0.99

**Table 4**  
Whole-rock Nd isotopic compositions for the Daura and Dutse rocks.

Sample	Rock Type	Age (Ma)	Sm (ppm)	Nd (ppm)	$^{147}\text{Sm}/^{144}\text{Nd}$	$^{143}\text{Nd}/^{144}\text{Nd}$	$2\sigma$	$\epsilon\text{Nd(t)}$	TDM (Ga)	$\text{T}^{\text{CDM2}} \text{ (Ga)}$	fSm/Nd
DA2	Daura amphibole syenite	324	11.3	59.6	0.116269	0.512529	0.000007	1.21	0.97	0.99	-0.41
DA3	Daura biotite granite	322	8.8	34.1	0.156056	0.512527	0.000006	-0.48	1.64	1.12	-0.21
DT2	Dutse fayalite syenite	232	11.1	52.8	0.116271	0.512590	0.000005	1.45	0.88	0.89	-0.41
DT4-1	Dutse arfvedsonite aegirine granite	263	39.8	207	0.127123	0.512371	0.000007	-2.86	1.37	1.27	-0.36

**Table 5**

Whole-rock Pb isotopic compositions for the Daura and Dutse rocks.

Sample	Rock Type	Zr (Ma)	$^{206}\text{Pb}/^{204}\text{Pb}$	$2\sigma$	$^{207}\text{Pb}/^{204}\text{Pb}$	$2\sigma$	$^{208}\text{Pb}/^{204}\text{Pb}$	$2\sigma$
DA2	Daura amphibole syenite	324	18.179	0.0002	15.566	0.0003	38.232	0.0005
DA3	Daura biotite granite	322	19.555	0.0004	15.634	0.0003	37.929	0.0008
DT2	Dutse fayalite syenite	232	18.352	0.0004	15.575	0.0003	38.690	0.0008
DT4-1	Dutse arfvedsonite aegirine granite	263	17.818	0.0003	15.544	0.0003	38.345	0.0008

over HREE [ $(\text{La/Yb})_N = 7.09\text{--}13.81$ ] and slight positive Eu ( $\text{Eu}/\text{Eu}^* = 1.17\text{--}1.36$ ) anomalies (Fig. 8b-d).

The Dutse arfvedsonite aegirine granite is characterized by pronounced enrichments in Nb, Ta, Pb, Zr and Hf with corresponding depletions in Ba, Sr, P and Ti (Fig. 8c). Notably, their Nb contents (91–207 ppm) are markedly higher than those of Daura and Dutse syenites (55–78 ppm). In the chondrite-normalized REE diagram (Fig. 8d), the arfvedsonite aegirine granite is enriched in LREE relative to OIB values and shows negative Eu anomalies ( $\text{Eu}/\text{Eu}^* = 0.18\text{--}0.19$ , Table 1), which is slightly lower than corresponding OIB values (Sun and McDonough, 1989). The Dutse arfvedsonite aegirine granite displays high LREEs, HREEs and HFSEs (i.e. Zr, Nb, and Ta) contents (Fig. 8c, d; Table 1), typical of the OIB-type peralkaline suites (Collins et al., 2019; Girei et al., 2019; Kinnaird, 1985).

The Daura biotite granite is characterized by relative enrichment of Nb, Ta, Pb, Zr and Hf but strong depletions of Ba, Sr, P and Ti (Fig. 8a). The Daura biotite granite shows higher Nb (136–149 ppm) and Th contents (70–71 ppm) than those of Daura and Dutse syenites (Nb = 55–78 ppm; Th = 7–8 ppm). In the chondrite-normalized REE diagram (Fig. 8b), the biotite granite is slightly depleted in LREE relative to OIB values and show strongly negative Eu anomalies ( $\text{Eu}/\text{Eu}^* = 0.02\text{--}0.03$ , Table 1).

Total REE concentrations in the Daura and Dutse syenites range from 261 to 354 ppm, lower than those of the Daura biotite granite (311–354 ppm) and Dutse arfvedsonite aegirine granite (924–988 ppm).

#### 4.3. Zircon U—Pb ages and trace elements

Results of LA-ICP-MS zircon U—Pb dating and zircon trace element analysis are listed in Table 2 and Supplementary Table S5, respectively. Zircon grains with low concordance (< 90%) were excluded from the following discussion and concordia plots. The zircons are mostly euhedral and typically 80 to 200  $\mu\text{m}$  in length. In the cathodoluminescence (CL) images, the zircon grains from the Daura and Dutse complexes are distinctly grey-dark black colour indicating variable thorium and uranium enrichment. Most zircon grains show faint oscillatory zoning patterns in CL images (Fig. 9a-d), indicating a magmatic origin.

Zircon grains from the Daura amphibole syenite show no obvious zoning but yield Th/U ratios ranging from 0.78–3.37 indicating a magmatic origin. 18 zircon spots show a  $^{206}\text{Pb}/^{238}\text{U}$  Concordia age (Fig. 9a) of  $324.4 \pm 0.7$  Ma (MSWD = 5.00), comparable to the weighted-mean  $^{206}\text{Pb}/^{238}\text{U}$  age of  $324.6 \pm 1.3$  Ma (MSWD = 0.85, n = 18, Fig. 9a). In the chondrite normalized plot, zircons from the Daura amphibole syenite are characterized by significant positive Ce and negative Eu anomalies further supporting a magmatic origin (Supplementary Table S5; Fig. 9 g). They are relatively enriched in ΣREE (6141–12,185 ppm; average = 7745 ppm) and Y (4213–19,626 ppm; average = 12,038 ppm) (Supplementary Table S5).

Zircon grains from the Daura biotite granite, on the other hand, show dark colour and weak zoning. A total of 19 zircon grains were analyzed for zircon U—Pb dating. However, most zircons from this sample contain high Th and U contents (up to 73,540 ppm and 21,833 ppm, respectively), resulting in discordant and meaningless ages (Table 2). Four concordant zircon grains with relatively apparent magmatic zonation (Fig. 9b) yield  $^{206}\text{Pb}/^{238}\text{U}$  Concordia age of  $322.5 \pm 3.4$  Ma (MSWD = 0.89, Fig. 9b) comparable to the weighted-

mean  $^{206}\text{Pb}/^{238}\text{U}$  age of  $322.4 \pm 6.7$  Ma (MSWD = 0.01, n = 4, Fig. 9b). There are another five low Th—U zircon data points that also give ages close to  $\sim 322$  Ma, even though the results are discordant and drift away from the isochron line (Fig. 9b). Further, the  $\sim 322$  Ma emplacement age of the Daura biotite granite closely overlap with the  $\sim 324$  Ma emplacement age of the Daura syenite. As a result, we interpret the  $\sim 322$  Ma age as reflective of the emplacement age of the biotite granite. In the chondrite normalized zircon REE pattern plot (Fig. 9 g), the Daura biotite granite shows a range of weak to strong positive Ce and negative Eu anomalies indicative of magmatic zircons. The zircon grains from the Daura biotite granite show moderate ΣREE (965–1343 ppm; average = 1213 ppm) and Y (880–1320 ppm; average = 1167 ppm) values (Supplementary Table S5).

Zircon grains from the Dutse fayalite syenite are dark to slightly bright with weak oscillatory zoning, characterized by variable Th/U values of 0.70–1.43. Calculated  $^{206}\text{Pb}/^{238}\text{U}$  Concordia age (Fig. 9c) of  $232.4 \pm 0.6$  Ma (MSWD = 0.14) was obtained from 15 zircon grains, comparable to the weighted-mean  $^{206}\text{Pb}/^{238}\text{U}$  age of  $232.4 \pm 1.2$  Ma (MSWD = 0.06, n = 15, Fig. 9c). In chondrite normalized zircon REE spider plots, apparently positive Ce and negative Eu anomaly (Fig. 9 h) indicating a magmatic origin for these zircons. The zircon grains from the Dutse fayalite syenite are relatively enriched in ΣREE (4162–7912 ppm; average = 6109 ppm) and Y (6623–14,842 ppm; average = 10,135 ppm) (Supplementary Table S5).

Zircon crystals from the Dutse porphyritic arfvedsonite aegirine granite are light grey with clear oscillatory zoning and narrow Th/U ratios (0.31–0.75). 13 zircon spots from the Dutse porphyritic arfvedsonite aegirine granite yield a  $^{206}\text{Pb}/^{238}\text{U}$  Concordia age (Fig. 9d) of  $263.6 \pm 2.8$  Ma (MSWD = 0.01), comparable to the weighted-mean  $^{206}\text{Pb}/^{238}\text{U}$  age of  $263.6 \pm 5.5$  Ma (MSWD = 0.79, n = 13, Fig. 9d). In the chondrite normalized zircon REE pattern plots, the zircons are characterized by prominent positive Ce and negative Eu anomalies (Fig. 9 h).

Zircon grains from the medium-coarse grained Dutse arfvedsonite aegirine granite show light grey zoned cores with Th/U values of 0.34–1.44. Analyzed zircon grains display an intercept age of  $230.2 \pm 5.3$  Ma (MSWD = 2.10, n = 15, Fig. 9e). Concordant grains display a  $^{206}\text{Pb}/^{238}\text{U}$  Concordia age (Fig. 9f) of  $232.0 \pm 1.5$  Ma (MSWD = 1.20), comparable to the weighted-mean  $^{206}\text{Pb}/^{238}\text{U}$  age of  $232.0 \pm 5.7$  Ma (MSWD = 2.70, n = 8, Fig. 9f). A single concordant zircon grain with a  $^{206}\text{Pb}/^{238}\text{U}$  age of 215 Ma is probably indicative of late-stage perturbation by hydrothermal fluids. In the chondrite normalized zircon REE pattern plots, positive Ce and negative Eu anomalies (Fig. 9 h) characterize zircons from the Dutse arfvedsonite aegirine granite. Compared to the zircons from the Dutse fayalite syenite, those from the Dutse arfvedsonite aegirine granite show variable ΣREE (355–4394 ppm; average = 1144 ppm) and Y contents (461–3284 ppm; average = 1427 ppm) (Supplementary Table S5).

#### 4.4. Zircon Lu—Hf isotopes

Zircon Lu—Hf isotopic compositions are listed in Table 3. Thirteen zircon spots of the Daura amphibole syenite yield  $^{176}\text{Hf}/^{177}\text{Hf}$  values of 0.2828–0.2830 and eHf(t) values of +7.8 to +16.7, corresponding to crustal model ages from 774 to 273 Ma. Seven zircon grain spots from the Daura biotite granite show  $^{176}\text{Hf}/^{177}\text{Hf}$  values of 0.2825–0.2826,

**Table 6**

Published age distribution data for alkaline ring complexes from Northern Niger to Nigeria (Data from Ahmed et al., 2021; Amuda et al., 2020; Bowden et al., 1976; Girei et al., 2019; Girei et al., 2020; Kamaunji et al., 2020; Karche and Vachette, 1978; Kinnaird, 1981; Moreau et al., 1994; Rahaman et al., 1984 and Van Breemen et al., 1975).

Province	Complex	Age	Method and Reference
Air Centre (Nth. Niger)	Adrar Bous (N20°20'; 9°00'E)	470 ± 5 Ma 429 ± 4 Ma	Rb-Sr Whole rock (Karche and Vachette, 1978) Rb—Sr Whole rock (Bowden et al., 1976)
Air Centre (Nth. Niger)	Tamgak (N19°03'; 8°40'E)	455 ± 19 Ma 414 ± 9 Ma	Single Rb/Sr whole-rock isochron (Karche and Vachette, 1978) Rb—Sr Isochron age (Moreau et al., 1994)
Air Centre (Nth. Niger)	Ofoud and Meuguer-Meuguer (N18°49'; 8°43'E)	409 ± 12 Ma	Rb/Sr Isochron age from 5 rocks (Moreau et al., 1994)
Air Centre (Nth. Niger)	Abontorok (N18°23'; 8°35'E)	399 ± 10 Ma	Rb/Sr Whole rock isochron (Karche and Vachette, 1978)
Air Centre (Nth. Niger)	Egalah (N18°06'; 8°48'E)	435 ± 8 Ma	Single Rb/Sr whole-rock isochron (Karche and Vachette, 1978)
Air Centre (Nth. Niger)	Aroyan and Azambardan-Tamoelet (N18°04'; 8°52'E)	426 ± 6 Ma	Single Rb/Sr whole-rock isochron (Karche and Vachette, 1978)
Air Centre (Nth. Niger)	Iskou (N18°10'; 8°42'E)	427 ± 20 Ma	Single Rb/Sr whole-rock isochron (Karche and Vachette, 1978)
Air Centre (Nth. Niger)	Taghouaji (N17°12'; 8°30'E)	407 ± 6 Ma 401 ± 5 Ma	Rb-Sr Whole rock (Karche and Vachette, 1978) Single Rb/Sr whole-rock isochron (Karche and Vachette, 1978)
Damagram-Mounio Centre (Sth. Niger)	Mounio and Goure (N13°35'; 10°10'E)	302 ± 5 Ma	7 point whole rock Rb/Sr Isochron (Bowden et al., 1976)
Damagram-Mounio Centre (Sth. Niger)	Tchouni-Zarniski (N14°08'; 9°34'E)	330 ± 3 Ma 302 ± 9 Ma	Rb/Sr syenite and granite whole-rock isochron (Karche and Vachette, 1978)
Damagram-Mounio Centre (Sth. Niger)	Zinder (N13°41'; 8°52'E)	330 ± 6 Ma	7 point whole rock Rb/Sr Isochron (Bowden et al., 1976)
Daura-Dutse Centre (Nth. Nigeria)	Daura (N12°55'; 8°31'E)	307 ± 13 Ma 324 ± 2 Ma	Quartz syenite whole rock Rb/Sr Isochron (Rahaman et al., 1984) Zircon U/Pb on syenites (This Study)
Daura-Dutse Centre (Nth. Nigeria)	Matsena (N13°10'; 10°10'E)	258 ± 5 Ma	Arfvedsonite whole rock Rb/Sr (Rahaman et al., 1984)
Daura-Dutse Centre (Nth. Central Nigeria)	Dutse (N11°44'; 9°21'E)	213 ± 7 Ma 263 ± 5 Ma 232 ± 6 Ma	Aegirine arfvedsonite granite Rb/Sr Isochron (Rahaman et al., 1984) Zircon U/Pb Aegirine Arfvedsonite granite (This study) Zircon U/Pb on Fayalite Syenites (This study)

**Table 6 (continued)**

Province	Complex	Age	Method and Reference
Jos-Bukuru Centre (Nth. Central Nigeria)	Shira (N11°30'; 10°04'E)	186 ± 5 Ma	Arfvedsonite granite Rb/Sr Isochron (Rahaman et al., 1984)
Jos-Bukuru Centre (Nth. Central Nigeria)	Dogo Dutse (N11°10'; 10°11'E)	213 ± 7 Ma	Aegirine arfvedsonite granite Rb/Sr Isochron (Rahaman et al., 1984)
Jos-Bukuru Centre (Nth. Central Nigeria)	Fagam (N11°06'; 10°02'E)	191 ± 3 Ma	Biotite granite Rb/Sr Isochron (Rahaman et al., 1984)
Jos-Bukuru Centre (Nth. Central Nigeria)	Nungi-Burra (N11°04'; 8°56'E)	183 ± 7 Ma	Riebeckite granite Rb/Sr Isochron (Rahaman et al., 1984)
Jos-Bukuru Centre (Nth. Central Nigeria)	Tibchi-Yelli (N11°06'; 10°02'E)	171 ± 3 Ma	Rb/Sr Isochron on biotite granite (Rahaman et al., 1984)
Jos-Bukuru Centre (Nth. Central Nigeria)	Ririwai (N10°44'; 8°44'E)	175 ± 5 Ma 171 ± 1 Ma	Rb/Sr isochron on aegirine-arfvedsonite granite (van Breemen et al., 1975) Zircon U/Pb on biotite granite (Girei et al., 2019)
Jos-Bukuru Centre (Nth. Central Nigeria)	Banke (N10°51'; 8°30'E)	173 ± 2 Ma	Rb/Sr Isochron on biotite granite (Rahaman et al., 1984)
Jos-Bukuru Centre (Nth. Central Nigeria)	Dutsen Wai (N10°55'; 8°13'E)	173 ± 2 Ma 175 ± 3 Ma	Rb/Sr Isochron on biotite granite (Rahaman et al., 1984) Zircon U/Pb of biotite granite (Amuda et al., 2020)
Jos-Bukuru Centre (Nth. Central Nigeria)	Kudaru (N10°37'; 8°26'E)	173 ± 3 Ma 180 ± 1 Ma 176 ± 2 Ma	Rb/Sr Isochron on biotite granite (Rahaman et al., 1984) Zircon U/Pb geochron on fayalite granite porphyry (Kamaunji et al., 2020) Zircon U/Pb geochron on biotite granite (Kamaunji et al., 2020)
Jos-Bukuru Centre (Nth. Central Nigeria)	Zaranda (N10°17'; 9°03'E)	199 ± 4 Ma 203 ± 1 Ma	Rb/Sr Isochron from 6 samples (van Breemen et al., 1975) Zircon U/Pb dating on syenites (Ahmed et al., 2021)
Jos-Bukuru Centre (Nth. Central Nigeria)	Jos-Bukuru (N9°40'; 8°46'E)	164 ± 4 Ma	7 point Rb/Sr isochron of biotite granite (van Breemen et al., 1975)
Jos-Bukuru Centre (Nth. Central Nigeria)	Shere (N10°02'; 9°07'E)	165 ± 2 Ma	Rb/Sr Isochron from 8 peralkaline granite samples (van Breemen et al., 1975)
Jos-Bukuru Centre (Nth. Central Nigeria)	Amo and Rukuba (N10°02'; 8°46'E)	165 ± 3 Ma	Rb/Sr Isochron on arfvedsonite granite sample (van Breemen et al., 1975)

(continued on next page)

Table 6 (continued)

Province	Complex	Age	Method and Reference
Jos-Bukuru Centre (Nth. Central Nigeria)	Ropp (N09°27'; 8°55'E)	161 ± 1 Ma 149 ± 2 Ma	Zircon U/Pb dating on pyroxene biotite granites (Vandi et al., unpubl)
			Zircon U/Pb dating on biotite granites (Amuda et al., 2020)
Jos-Bukuru Centre (Nth. Central Nigeria)	Sara-Fier and Pankshin (N9°14'; 9°38'E)	154 ± 4 Ma	Rb/Sr Isochron on arfvedsonite granite sample (van Breemen et al., 1975)
Jos-Bukuru Centre (Nth. Central Nigeria)	Mada (N8°46'; 8°25'E)	150 ± 2 Ma 152 ± 1 Ma	Rb/Sr Isochron on biotite granite sample (Rahaman et al., 1984)
			Zircon U/Pb dating on biotite granite sample (Girei et al., 2020)
Jos-Bukuru Centre (Nth. Central Nigeria)	Afu (N8°30'; 7°48'E)	141 ± 1 Ma	Rb/Sr Isochron on biotite granite sample (Kinnaird, 1981)

$\epsilon\text{Hf(t)}$  values of +0.2 to +1.2 and  $T_{\text{DM2}}$  (Crustal) ages of 1263–1325 Ma.

Twelve zircon crystals from the Dutse fayalite syenite yield  $^{176}\text{Hf}/^{177}\text{Hf}$  values of 0.2827–0.2828,  $\epsilon\text{Hf(t)}$  values of +3.8 to +5.4 and  $T_{\text{DM2}}$  age of 833–923 Ma. Ten zircon grains of the Dutse arfvedsonite aegirine granite yield  $^{176}\text{Hf}/^{177}\text{Hf}$  ratios of 0.2825–0.2826,  $\epsilon\text{Hf(t)}$  values of −1.2 to −3.1 and  $T_{\text{DM2}}$  age of 1367–1486 Ma. Equally, 10 zircon spots from the Dutse porphyritic arfvedsonite aegirine granite yielded  $^{176}\text{Hf}/^{177}\text{Hf}$  ratios of 0.2825–0.2826,  $\epsilon\text{Hf(t)}$  values of −1.8 to −3.8 and  $T_{\text{DM2}}$  age of 1385–1477 Ma.

#### 4.5. Whole-rock Sm—Nd isotopes

Whole-rock Sm—Nd isotopic compositions are listed in Table 4. Calculations of  $\epsilon\text{Nd(t)}$ ,  $T_{\text{DM1}}$  and  $T_{\text{DM2}}$  are based on initial  $^{147}\text{Sm}/^{144}\text{Nd}$  and  $^{143}\text{Nd}/^{144}\text{Nd}$  ratios of 0.1162 and 0.5125 for the Daura amphibole syenite, and of 0.1560 and 0.5125 for the Daura biotite granite. Corresponding ratios for the Dutse arfvedsonite aegirine granite are 0.1271 and 0.5123, and 0.1162 and 0.5125 for the Dutse fayalite syenite. Zircon U—Pb weighted ages for the rock units in this study are used for  $\epsilon\text{Nd(t)}$  calculations. The  $\epsilon\text{Nd(t)}$  values are +1.5 and +1.2, respectively for the Dutse and Daura syenites, −2.9 for the Dutse arfvedsonite aegirine granite, and −0.5 for the Daura biotite granite. The  $f\text{Sm/Nd}$  values in the Daura amphibole syenite, Daura biotite granite, Dutse fayalite syenite and Dutse arfvedsonite aegirine granite are −0.41, −0.21, −0.41, and −0.36, respectively. Two-stage modal ages ( $T_{\text{DM2}}$ ) for the Daura amphibole syenite, Dutse fayalite syenite and Dutse arfvedsonite aegirine granite are 990 Ma, 890 Ma and 1270 Ma, respectively.

#### 4.6. Whole-rock Pb isotopes

The whole-rock Pb isotopic ratios of the analyzed samples are shown in Table 5. The  $^{206}\text{Pb}/^{204}\text{Pb}$  ratios for the Daura amphibole syenite, Daura biotite granite, Daura fayalite syenite and Dutse arfvedsonite aegirine granite are 18.179, 19.555, 18.352, and 17.818, respectively. Correspondingly, the  $^{207}\text{Pb}/^{204}\text{Pb}$  ratios are 15.566, 15.634, 15.575, and 15.544, respectively, and the  $^{208}\text{Pb}/^{204}\text{Pb}$  ratios are 38.232, 37.929, 38.690, and 38.345, respectively.

## 5. Discussion

### 5.1. The onset time and age migration of the anorogenic alkaline magmatism in the NaYG province

Zircon U—Pb dating from this study allows for new constraints on the timing of the Daura and Dutse complexes and the transition time of the post-Cambrian alkaline magmatism from the NrYG to the NaYG provinces. Based on our results, the Daura amphibole syenite crystallized at  $324 \pm 1$  Ma and the Daura biotite granite at  $\sim 322$  Ma. Although they roughly overlap (within error range) with previously reported whole-rock Rb—Sr age (307 ± 13 Ma; Rahaman et al., 1984), these ages (324–322 Ma) provide more precise geochronological data for the Daura complex.

Previous studies generally documented the beginning of the anorogenic magmatism in Nigeria as a Late Triassic event with the emplacement of the Dutse complex (213 Ma; whole-rock Rb—Sr age; Kinnaird, 1981; Rahaman et al., 1984). Our zircon U—Pb ages from the Daura complex record the earliest post-Cambrian anorogenic magmatism in the northernmost NaYG province ( $\sim 324$  Ma). These data help us to reconstruct the onset time of the post-Cambrian anorogenic magmatism in the NaYG as a Late Carboniferous event. To the north, our new age data of the Daura complex (324–322 Ma) connect well with the Zinder (323 Ma; Rahaman et al., 1984) and Tchouni-Zarniski alkaline complexes (320 Ma; Rahaman et al., 1984) in the southern NrYG province.

The Dutse complex sites southward of the Daura complex, representing the northernmost anorogenic alkaline complex of the northcentral NaYG province (Fig. 1a). Our results show that the Dutse porphyritic arfvedsonite aegirine granite, arfvedsonite aegirine granite and fayalite syenite yield  $263 \pm 3$  Ma,  $232 \pm 2$  Ma and  $232 \pm 1$  Ma, respectively (Fig. 9b-d). These data suggest that the Dutse complex is a product of episodic magmatic events. The younger age (232 Ma) is roughly consistent with previous whole rock Rb—Sr age of the Dutse complex (213 Ma; Kinnaird, 1981), while the older age (263 Ma) closely matches the reported whole rock Rb—Sr ages for the Matsena complex in northern NaYG (258 ± 5 Ma; Table 6; Rahaman et al., 1984). Therefore, the new zircon dating data indicate that the alkaline magmatism in the northcentral NaYG province began in the Middle Permian (263 Ma) rather than the Late Triassic (213 Ma).

Previous whole rock Rb—Sr dating results have established a general N-S decreasing age trend in the Niger-Nigeria alkaline province, with the oldest alkaline magmatism preserved in Air Massif of the northern NrYG province (470–401 Ma) followed by the Zinder-Mounio centre of southern NrYG province (330–302 Ma), the Daura-Matsena centre of northern NaYG province (313–258 Ma) and the Jos-Bukuru centre of northcentral NaYG province (213–141 Ma) (Figs. 1a & 10a; Table 6). Recent zircon U—Pb dating work on the Ririwai, Kudaru, Mada, Ropp and Zaranda complexes mostly match previous whole rock Rb—Sr dating results (Ahmed et al., 2021; Amuda et al., 2020; Girei et al., 2019, 2020; Kamaunji et al., 2020) and confirm the existence of the age migration trend in the NaYG province (Fig. 1b; Table 6). Our new data from the Daura and Dutse complexes update the onset time of the alkaline magmatism in northern and northcentral NaYG provinces and provide a perfect age connection between the NaYG and NrYG provinces. From a broad view, all the dating results (including both whole-rock Rb—Sr and zircon U—Pb dating results) show a main N-S age migration trend for the emplacement of alkaline centres in northern Niger to northcentral Nigeria (Fig. 10). In the northern NrYG, the parallel N-S trend traces a southward migration from the Adrar Bous (470 Ma) to the Taghouaji (401 Ma) complex (Fig. 10b). In the southern NrYG and northern NaYG region, a rough N-S trend is traced from the Zinder (330 Ma) to Matsena (258 Ma) complexes (Fig. 10c). In the northcentral NaYG, alkaline centres aligned in an ENE-WSW direction from the Dutse complex (263 Ma) through the Jos-Bukuru centre (164 Ma) to the Afu centre (141 Ma) (Fig. 10d). Besides, an E-W age

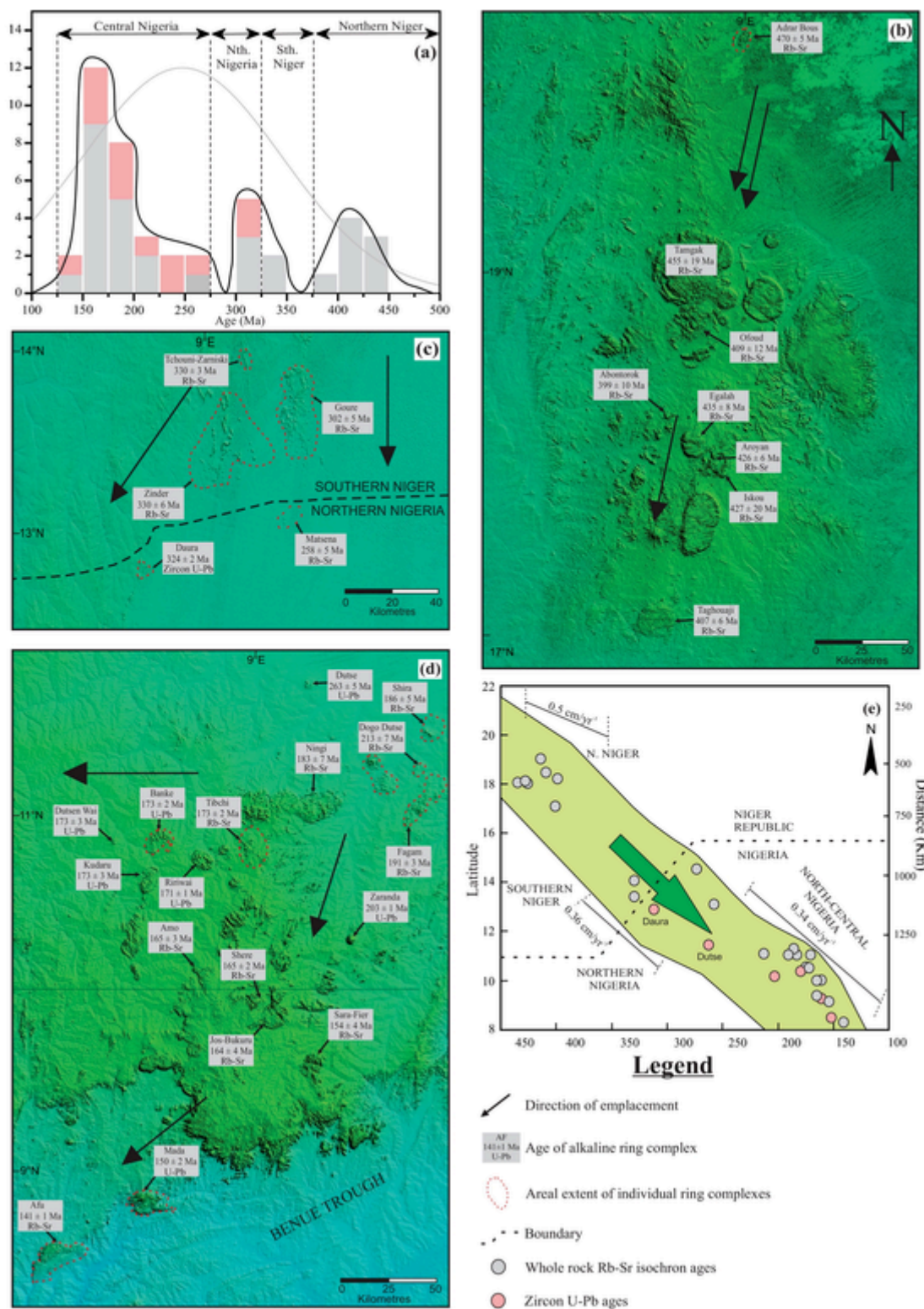


**Fig. 10.** Histograms of (a) Zircon U—Pb zircon and whole-rock Rb—Sr ages from the Niger-Nigeria alkaline complexes. Age and distribution trend maps for alkaline ring complexes of the Niger-Nigeria province (b) northern Niger, (c) northern Nigeria, (d) northcentral Nigeria, and (e) Distance vs age variation trend for the alkaline province.

migration trend is likely present as well from the Fagam (191 Ma) through Ningi (183 Ma) to Dutsen Wai complexes (173 Ma) in the northcentral NaYG (Fig. 10d). Migration rates in the sub-provinces of the Niger-Nigeria alkaline belt was calculated from lateral extent of sub-province divided by total migration time recorded in each sub-province (Fig. 10c). Overall, stepwise age trends for the Niger-Nigeria

alkaline granite province shows unequal migration rates per  $\text{cm}/\text{yr}^{-1}$  from the northern Niger to the northcentral Nigerian centres. Calculated migratory rates for the northern NrYG, southern NrYG to northern NaYG and the northcentral NaYG centres are 0.5 cm/yr, 0.36 cm/yr and 0.34 cm/yr, respectively (Fig. 10e).

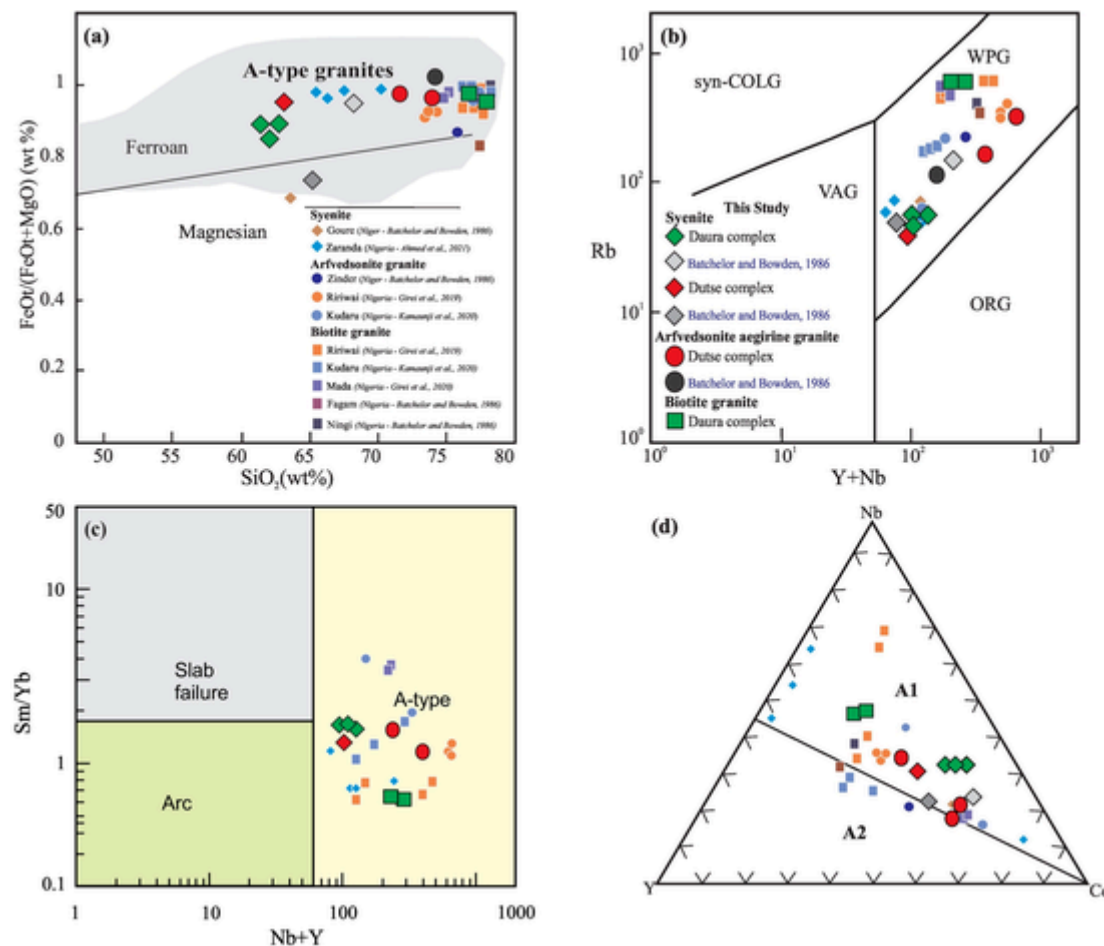


**Fig. 11.** Chemical and tectonic discrimination plots for atypical A-type granitoids. (a)  $\text{FeOt}/(\text{FeOt} + \text{MgO})$  (wt %) versus  $\text{SiO}_2$  (after Frost and Frost, 2001), (b) Rb versus  $\text{Y} + \text{Nb}$ , (c)  $\text{Sm}/\text{Yb}$  versus  $\text{Nb} + \text{Y}$ , and (d) Binary and ternary trace element geochemical discrimination diagram for A-type granite (after Eby, 1992). Data of granites plotted for comparisons are from Bachelor and Bowden (1986), Girei et al. (2019, 2020) and Kamaunji et al. (2020).

## 5.2. Petrogenesis of the Daura-Dutse syenites

### 5.2.1. Magma source of the Daura-Dutse syenites

The Daura and Dutse granitoids are all weakly peraluminous to peralkaline. They have high HFSE contents ( $\text{Zr} + \text{Nb} + \text{Ce} + \text{Y} > 1000$  ppm), elevated alkali oxides ( $\text{Na}_2\text{O} + \text{K}_2\text{O}$ ) and high Ga/Al ratios and show depletion in  $\text{CaO}$ ,  $\text{MgO}$  and  $\text{P}_2\text{O}_5$ , typical of “A-type” granites (Eby, 1992; Collins et al., 2019; Fig. 11a-d). On the Nb-Y-Ce ternary granite classification plot (Eby, 1992), the Daura and Dutse plutonic suites mostly plot within the A<sub>1</sub> field with the Dutse arfvedsonite aegirine granite straddling the A<sub>1</sub>/A<sub>2</sub> field (Fig. 11d). A-type granite worldwide has commonly been proposed to be generated from metasomatized lithospheric mantle (Collins et al., 2019), meta-mafic lower crust (Lubala et al., 1994), and a mixture of both mantle and crustal materials (Yang et al., 2006). Whilst A<sub>1</sub>-type suites are mostly originated from a mantle source in an intra-plate anorogenic setting (Dickin et al., 1991; Eby, 1992).

The Daura amphibole syenite and Dutse fayalite syenite both have positive  $\epsilon_{\text{Nd}}$  (t) values of +1.2 and +1.5, respectively. The Nd isotopic characteristics of the syenites are similar to a set of cumulate leucogabbro-microgabbro phases ( $\epsilon_{\text{Nd}}(\text{t}) = +0.6$  to +1.8) suites in the Silurian Ofoud-Taguei complex (420 Ma) in the northern NrYG (DeMaiffe et al., 1991) and the syenite ( $\epsilon_{\text{Nd}}(\text{t}) = +0.9$ ) from the Zaranda complex (203 Ma) in the northcentral NaYG (Dickin et al., 1991). These syenite-leucogabbro suites express overlapping mantle signatures with Mesozoic basalts ( $\epsilon_{\text{Nd}}(\text{t}) = +0.7$  to +7.2) from the Benue trough in eastern Nigeria (Halliday et al., 1988). The  $\epsilon_{\text{Nd}}(\text{t})$  val-

ues of the studied syenites are markedly higher than the  $\epsilon_{\text{Nd}}(\text{t})$  values of the Pan-African (-10.4 to -20.5) and Paleoproterozoic basement rocks (-11.7 to -26.9) from northcentral Nigeria (Dickin et al., 1991). These results rule out partial melting of crustal rocks as a source for the syenitic magmas. Initial Nd ratios and  $^{206}\text{Pb}/^{204}\text{Pb}$  isotopic signatures for the syenitic units in the Daura (0.5125 and 18.179) and Dutse suites (0.5126 and 18.352) are also less radiogenic than those of the Pan-African granites & basement rocks (0.5113–0.5121 and 17.120–19.660) (Dickin et al., 1991). These values further rule out the derivation of the parental melts for the Daura-Dutse suites (Fig. 12b) primarily from crustal melting of country rocks as proposed by other workers (Bowden, 1985; Martin, 2006). Although the  $\epsilon_{\text{Nd}}(\text{t})$  results of the syenites imply a depleted mantle-source, the Pb isotopic data plot near the EMII field (Fig. 12c, d), implying an EMII mantle source as the parental magma. In contrast, the  $\epsilon_{\text{Hf}}(\text{t})$  values display extremely positive values (+7.8 to +16.7 and +3.8 to +5.4 for the Daura and Dutse syenites, respectively), reflecting generation from depleted mantle-derived melts as well. In addition to the isotopic data, the Daura-Dutse syenitic suites are characterized by a narrow range of Th/Ta values (1.87–2.20) which is broadly similar to those from mantle-derived sources (~2; Shellnutt et al., 2009). Likewise, Nb/Ta values of the studied syenites (15–23) are well above average continental crust (8–14) values and are more reflective of derivation from OIB-like mantle sources (15.9 ± 0.6; Pfander et al., 2007). Furthermore, the syenites show high Nb/U ratios (39–42) similar to ocean-island basalt (47.1) and higher than average continental crustal (<25) values (Sun and

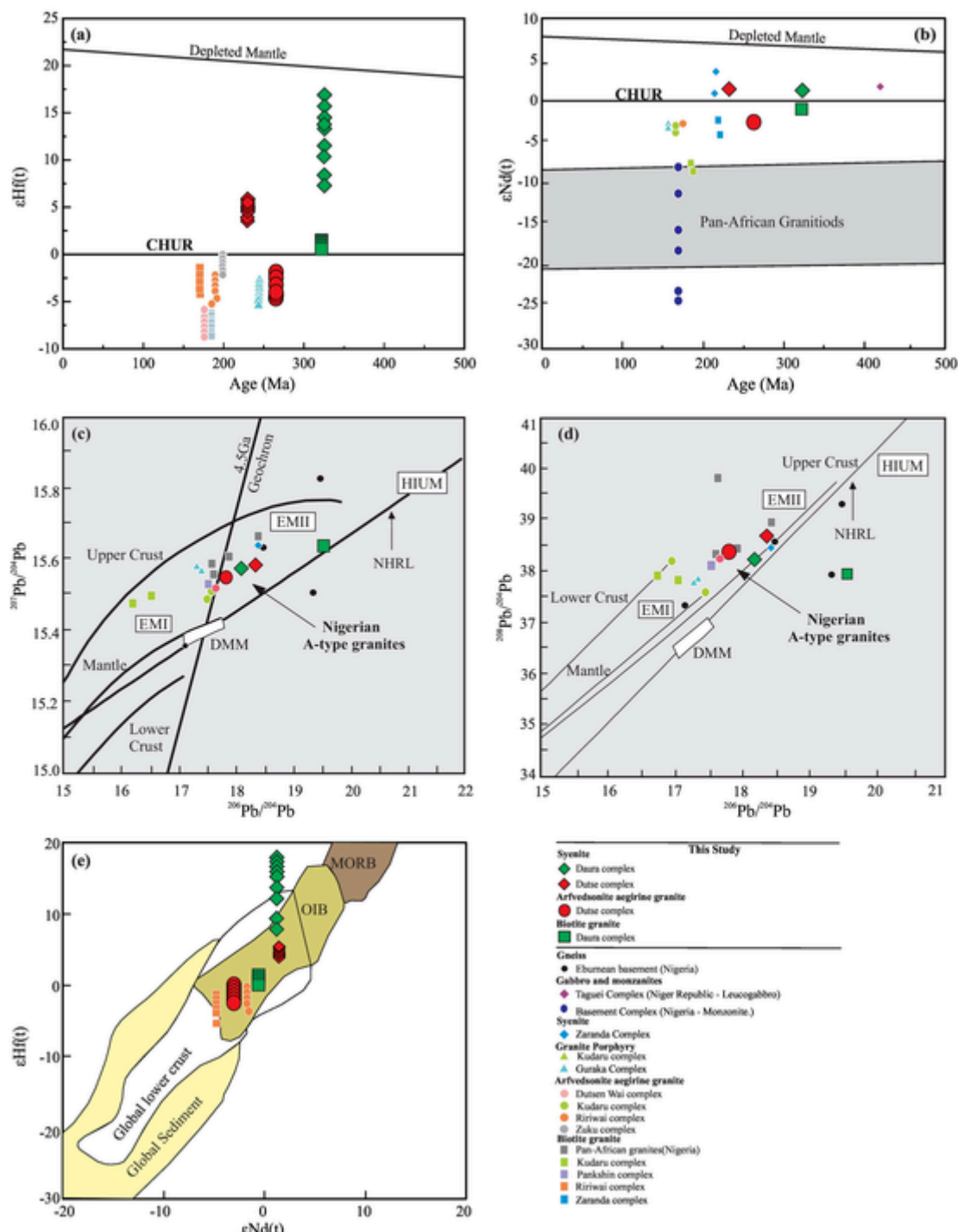


**Fig. 12.** Isotopic diagrams of the Daura-Dutse granites. (a)  $\epsilon\text{Hf(t)}$  versus age (Ma) diagram, (b)  $\epsilon\text{Nd(t)}$  against age (Ma) diagram, (c)  $^{207}\text{Pb}/^{204}\text{Pb}$  versus  $^{206}\text{Pb}/^{204}\text{Pb}$ , and (d)  $^{208}\text{Pb}/^{204}\text{Pb}$  versus  $^{206}\text{Pb}/^{204}\text{Pb}$  (modified from Zindler and Hart 1986), and (e)  $\epsilon\text{Hf(t)}$  vs.  $\epsilon\text{Nd(t)}$ . CHUR: Chondrite Universal, DMM: depleted member, EM I: enriched mantle type I; EM II: enriched mantle type II; MORB: mid-ocean ridge basalt; PREMA: prevalent mantle (primitive mantle segment); HIMU: high U/Pb (U/Th) mantle; BSE: proverbial bulk silicate Earth (after Zindler and Hart, 1986).  $\epsilon\text{Hf(t)}$  and  $\epsilon\text{Nd(t)}$  data taken for comparison from Ahmed et al. (2021), Amuda et al. (2020), Girei et al. (2019), Kamaunji et al. (2020) and Vincent et al. (Unpublished data).  $\epsilon\text{Nd(t)}$  data for Nigerian Pan-African basement complex of isotope ratios at 170 Ma are from Dickin et al. (1991) and estimated values of  $\epsilon\text{Hf(t)}$  and  $\epsilon\text{Nd(t)}$  for global lower crust and sediment were taken from Wang et al. (2016).

McDonough, 1989), further suggesting that their parental magmas is unlikely to be of crustal origin.

#### 5.2.2. A cumulate genesis for the Daura-Dutse syenites?

The Daura and Dutse syenites both contain >60% feldspars, display positive chondrite-normalized Eu anomalies ( $\text{Eu}/\text{Eu}^* \geq 1$ ; Table 1) and positive primitive mantle-normalized Ba anomalies, indicative of alkali

feldspar cumulate rocks (Shellnutt, 2021). In particular, the Daura amphibole syenite show typical cumulate textures with anhedral mafic minerals filling the gaps between coarse, interconnected euhedral feldspars (Fig. 2a). The  $\epsilon\text{Hf(t)}$  values (+7.8 to +16.7) of the Daura amphibole syenite are also much higher than the Dutse fayalite syenite (+3.8 to +5.4) and other granites (-3.8 to +1.2) and decoupled from whole rock  $\epsilon\text{Nd(t)}$  data (+1.2). These signatures along with cumulate

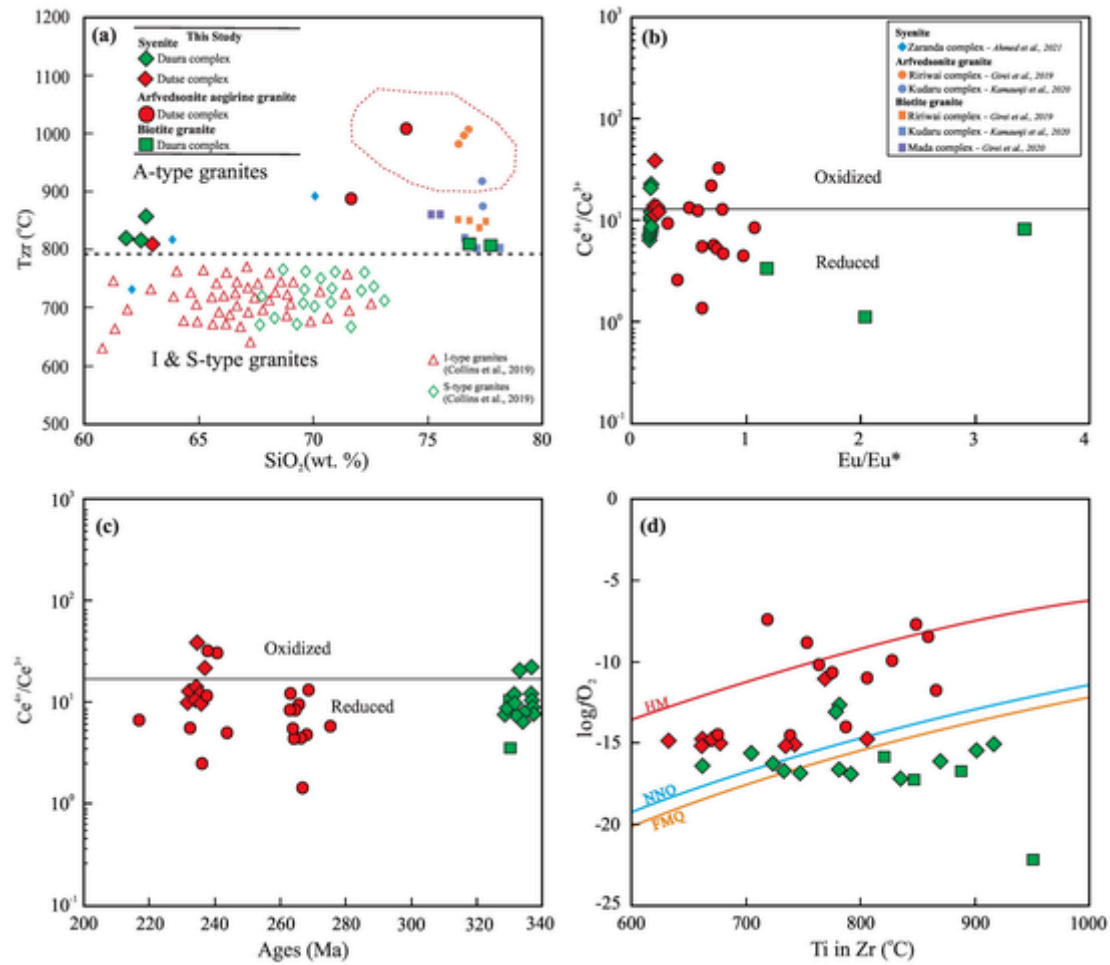


**Fig. 13.** Trace element variation plots for petrogenetic differentiation. (a)  $\text{SiO}_2$  vs  $T_{\text{zr}}$  ( $^{\circ}\text{C}$ ). Dashed red line represents cluster of high temperature peralkaline granites (see text for discussion), (b)  $\text{Ce}^{4+}/\text{Ce}^{3+}$  versus  $\text{Eu}/\text{Eu}^*$  for the Daura and Dutse complexes, (c)  $\text{Ce}^{4+}/\text{Ce}^{3+}$  versus Age (Ma) for the Daura and Dutse complexes, and (d)  $\log f_{\text{O}_2}$  versus  $T$  in zircon/ $^{\circ}\text{C}$  for the Daura and Dutse complexes. Parameters for b-d were computed from zircon composition. Note: NNO = nickel-nickel oxide buffer, FQM = fayalite-quartz-magnetite buffer, Hm = hematite buffer, and IW = iron-wüstite buffer. Plotted zircon data are only for concordant ( $> 90\%$ ) data points. Data of granites plotted for comparisons are from Batchelor and Bowden (1986), Girei et al. (2019, 2020) and Kamaunji et al. (2020). (For interpretation of the references to colour in this figure legend, the reader is referred to the web version of this article.)

textures observed in hand specimens further imply magma accumulation process, involving an early crystallization of accessory zircon from a depleted initial melt. Likewise, the low F (0.02–0.10 wt%) and  $\text{Na}_2\text{O}$  (0.03–0.14 wt%) contents of the biotite from the Daura syenite are markedly different from the biotite of the Daura and Dutse granites, suggesting early crystallization of biotite. Similar evidences are also observed in the Si- and Na-poor and Ca-rich amphiboles from the Daura amphibole syenites. Therefore, we postulate that the Daura amphibole syenite might represent a feldspar-rich cumulate rock. As mentioned above, the Daura amphibole syenite has a very similar  $\epsilon\text{Nd(t)}$  results with the leucogabbros from the NtYG province, which also display positive Eu anomalies and have been considered as cumulate rocks (DeMaiffe et al., 1991). It is likely that the Daura syenite was produced by crystal accumulation of a residual silicic melt that derived from a mafic parental magma and experienced separation of plagioclase-rich cumulate phases. A similar syenite cumulate rock has been reported in the Emeishan LIP (Shellnutt, 2021; Shellnutt et al., 2009).

Although, positive chondrite-normalized Eu anomalies and positive primitive mantle-normalized Ba anomalies are also recorded in the Dutse fayalite syenite, other evidences synonymous with the Daura cumulate syenite are lacking in the Daura fayalite syenite. For example, the feldspar proportion is smaller and a typical cumulate texture is not clear in hand specimen photomicrographs of the Dutse fayalite syenite (Fig. 2d). Furthermore, Nd—Hf isotopic decoupling is also not as ap-

parent as in the Daura amphibole syenite. It is likely that the weak positive Eu anomalies and Ba anomalies in the Dutse syenite (Fig. 4d) result from excess feldspar in the less evolved melts from which the syenitic suites are derived, similar to syenitic suites from the Okenyanya igneous complex in northern Namibia (Watkins and le Roex, 1991).

### 5.3. Petrogenesis of the Daura-Dutse granites

In comparison to the syenitic rocks, the  $\epsilon\text{Nd(t)}$  results of the Daura biotite granite ( $\epsilon\text{Nd(t)} = -0.5$ ) and Dutse arfvedsonite aegirine granite ( $\epsilon\text{Nd(t)} = -2.9$ ) are obviously lower (Fig. 12b). These Nd isotopic signatures overlap the reported values of other biotite granites ( $\epsilon\text{Nd(t)} = -1.3$  to  $-9.2$ ) and arfvedsonite aegirine granites ( $\epsilon\text{Nd(t)} = -1.9$  to  $-4.2$ ) in the northcentral NaYG province (Dickin et al., 1991; Girei et al., 2019; Kamaunji et al., 2020). The Pb-isotopes of the Daura biotite granite and Dutse arfvedsonite aegirine granite are similar to the Daura and Dutse syenites as well as other alkaline granitoids from the NaYG province, plotting between the EMI and EMII fields (Fig. 12c, d). The Nd—Pb isotopic signatures of the Daura biotite granite and Dutse arfvedsonite aegirine granite are markedly higher than those Pan-African granites and Precambrian basement suites from northcentral NaYG (Dickin et al., 1991), ruling out the derivation of the NYG granite primarily from partial melting of local country rocks. Zircon  $\epsilon\text{Hf(t)}$  values of the Dutse arfvedsonite aegirine granite ( $-1.2$  to  $-3.8$ ) and Daura bi-

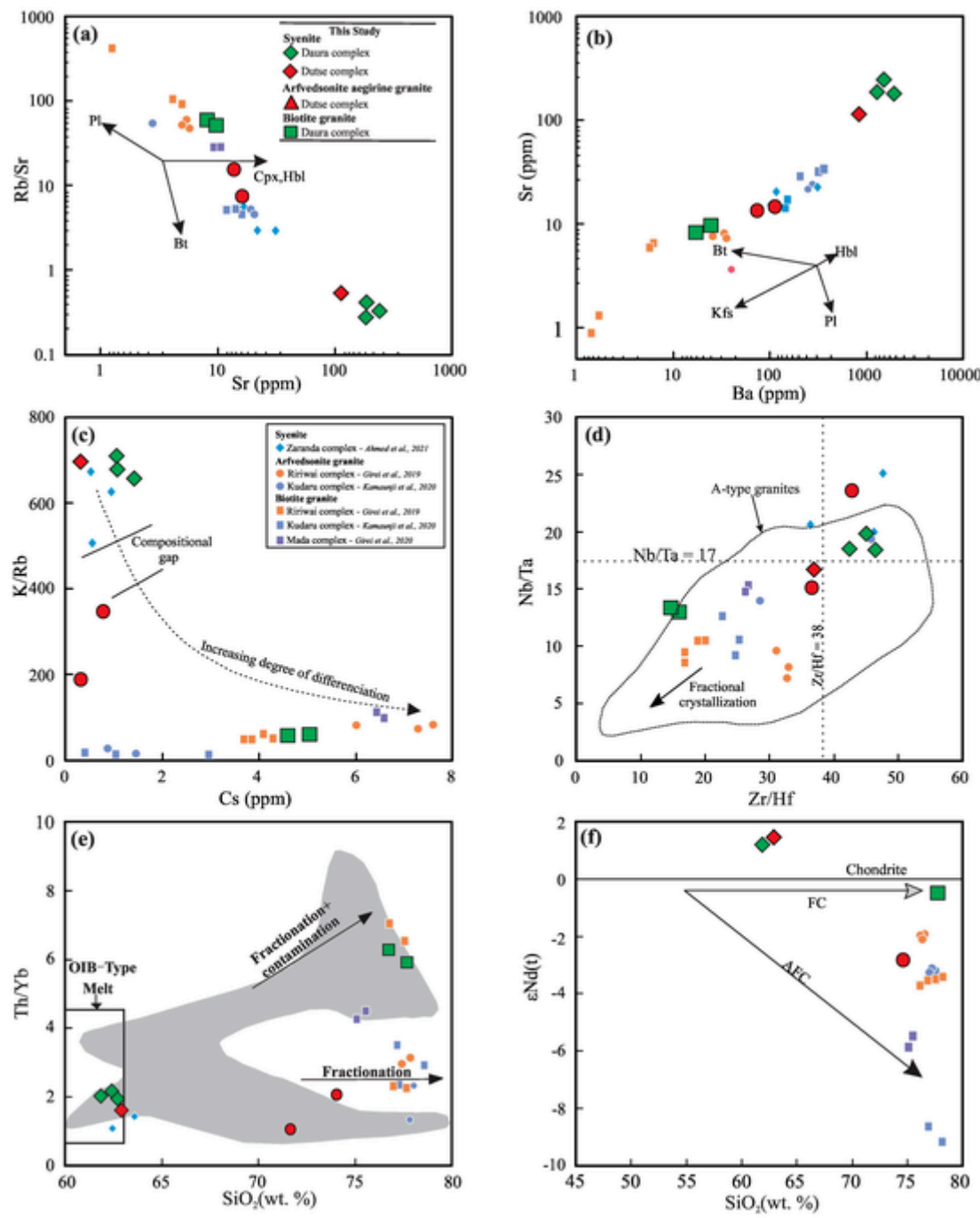


**Fig. 14.** Whole-rock geochemical diagrams for petrogenetic differentiation. (a) Rb/Sr vs. Sr, (b) Sr vs. Ba, (c) K/Rb vs. Cs, (d) Zr/Hf vs. Nb/Ta, (e) Th/Yb vs. SiO<sub>2</sub>, and (f) SiO<sub>2</sub> vs.  $\epsilon$ Nd(t). Data of granites plotted for comparisons are from Batchelor and Bowden (1986), Girei et al. (2019, 2020) and Kamaunji et al. (2020).

otite granite (+0.2 to +1.2) are apparently lower than those of the syenitic rocks but similar to those of other alkaline granitoids from the NaYG province (Fig. 12a). The  $\epsilon$ Hf (t) values from these rocks are well above values from Pan-African granitoids and basement complexes of Nigeria and West Africa ( $\epsilon$ Hf (t) = -3.1 to -20.8; Bute et al., 2019; Ganade et al., 2016). Our combined whole-rock Nd—Pb and zircon Lu—Hf isotopes suggest crustal contamination of a mantle-derived melt or mixing of crustal derived and mantle-derived melts for the origin of the Daura-Dutse granites. However, we favor variable crustal contamination of mantle-derived magmas for the petrogenesis of the Daura-Dutse granites. Isotopic values from the Daura-Dutse granites ( $\epsilon$ Hf(t) = -3.8 to +1.2; up to  $\epsilon$ Nd(t) = -2.9) are markedly different from signatures seen in NaYG complexes (e.g. the Mada and Ningi com-

plex) derived from mixing of crustal and mantle-derived melts ( $\epsilon$ Hf (t) = -5.0 to -10.3,  $\epsilon$ Nd(t) = -5.9; Girei et al., 2020, Vincent et al., 2021), suggesting limited to moderate contribution from crustal sources for the origin of the Daura-Dutse granites. Furthermore, the Daura biotite granite and Dutse arfvedsonite aegirine granite show moderately high ratios of Nb/Ta (12.97–23.62; average = 16.26) and Zr/Hf (14.68–42.73; average = 27.47; Table 1). These values are close to or slightly lower than the estimated mantle Nb/Ta (17.5; Green, 1995) and Zr/Hf ratios (35–45; Wedepohl, 1995) and markedly higher than crustal ratios (Nb/Ta = 8–14; Zr/Hf < 25), further implying that these rocks were most likely sourced from mantle-derived magmas with moderate contribution from crustal material.

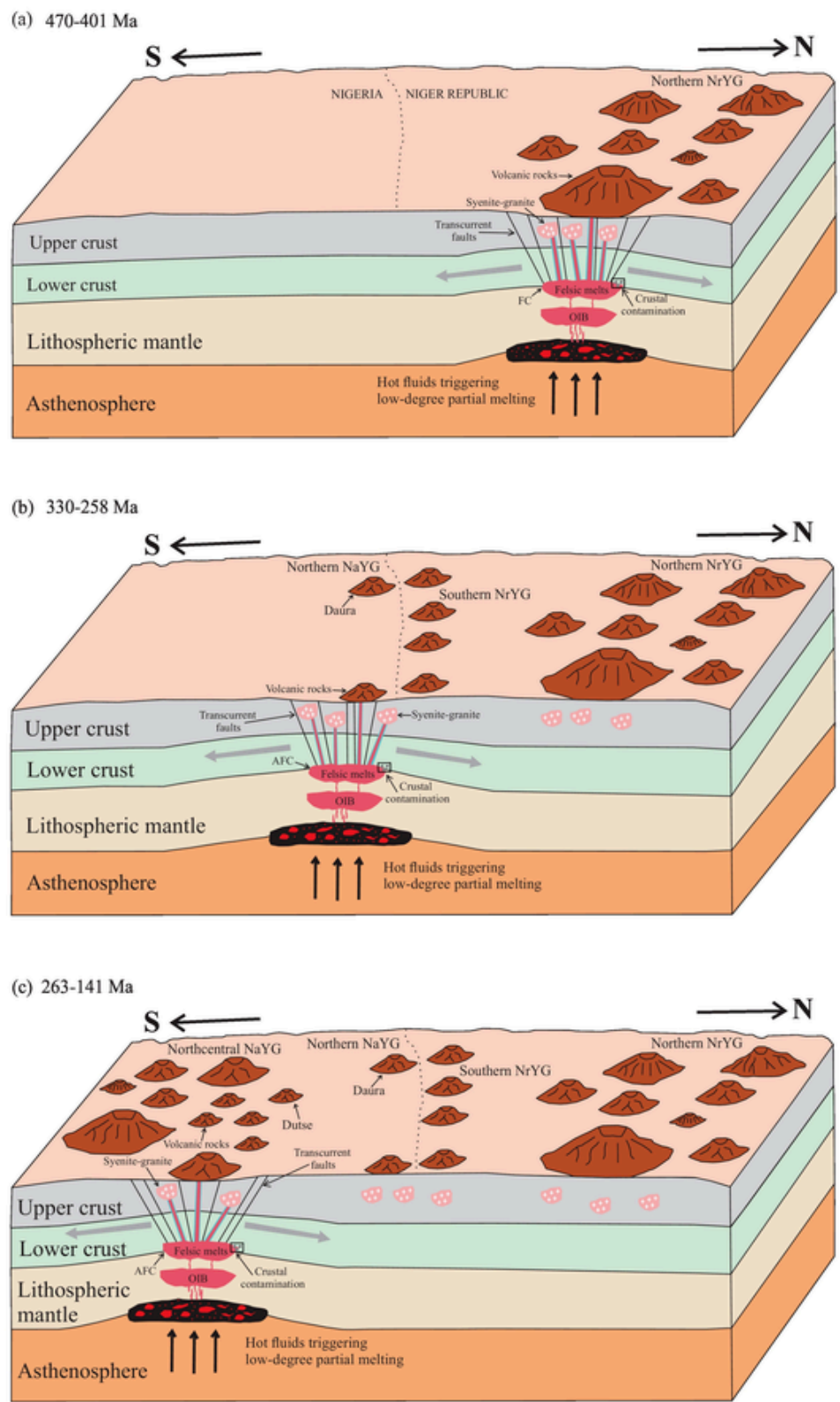


**Fig. 15.** A three stage tectonic model for the emplacement of alkaline intrusive complexes in the Niger-Nigeria province (a) northern NrYG, (b) southern NrYG-northern NaYG, and (c) northcentral NaYG.

The Daura and Dutse granites are temporally and spatially associated with the Daura and Dutse syenites, indicating their close genetic relationships. Combined with their isotopic variations, it is likely that assimilation and fractional crystallization (AFC) processes of non-cumulate syenitic magmas generated the granitic rocks. Suppose the

Daura amphibole syenite represents the alkaline feldspar cumulates, the other rocks might reflect the evolved products of the residual melt which underwent variable degrees of AFC processes. For the Daura biotite granites, a slight decoupling is recorded in zircon Lu—Hf ( $\epsilon_{\text{Hf}}(t) = +0.2$  to  $+1.2$ ) and whole-rock Sm—Nd ( $\epsilon_{\text{Nd}}(t) = -0.5$ ) iso-

topic signatures. The positive zircon Lu—Hf isotope values likely reflects initial isotopic characteristics of mantle-derived melts forming the Daura biotite granites due to the earlier crystallization of zircon, while, whole-rock Sm—Nd isotope values reflect moderate crustal contamination of the primary mantle-derived melts and support assimilation and fractional crystallization (AFC) processes for the evolution of the Daura biotite granites. From the Dutse fayalite syenite to the Daura and Dutse granites, the calculated differentiation indexes (DI) obviously increase from 86 to 88–97 (Table 1). The variation trends of some major elements (e.g., CaO and TiO<sub>2</sub>; Table 1) as well Sr, Ba and P (Fig. 7a–e) imply fractionation of calcic amphiboles, K-feldspars and Fe—Ti oxide as well as apatite during magma evolution. The negative correlations of Al<sub>2</sub>O<sub>3</sub> and Sr with SiO<sub>2</sub> (Fig. 6a, f), Rb/Sr vs Sr and Ba vs Sr plots (Fig. 14a, b) indicate that the fractionation of plagioclase plays a major role during magma evolution. The magma evolution process is also traced by the whole rock K/Rb, Nb/Ta and Zr/Hf ratios (Fig. 14c–d). The decreasing CaO and MgO and increasing SiO<sub>2</sub> and Na<sub>2</sub>O of pyroxene from the Dutse fayalite syenite to the arfvedsonite granite also trace increasing magma differentiation from the least evolved syenite to the evolved granite (Fig. 3f; Supplementary Table S4). The Fe<sup>3+</sup> and Na<sup>+</sup>-rich rims of clinopyroxene from the Dutse fayalite syenite (Fig. 5g, l) further record this process. In addition, Ce/Pb ratios of the Daura biotite granite and the Dutse arfvedsonite aegirine granite (6–35, mean of 13) vary between the values of mantle- and crust-derived magmas (25 and 4, respectively), further suggesting AFC processes for the evolution of these rocks (Zhu et al., 2020).

#### 5.4. Physical properties of the magmas

Whole-rock zircon saturation thermometry (Tzr) (after Gervasoni et al., 2016) and Ti-in-zircon geothermometry (after Watson and Harrison, 2005) are applied here to constrain the magma temperature of the Daura and Dutse complexes (Collins et al., 2019). Calculated Tzr values are between 809 and 856 °C for the Daura and Dutse syenites, 805–806 °C for the Daura biotite granite and 888–1008 °C for Dutse arfvedsonite aegirine granites (Table 1). According to our results, the Daura-Dutse alkaline suites all have high Tzr temperatures (Avg: > 800 °C), similar to those of A-type granites and much higher than temperatures typical in S- and I-type granitoids (< 800 °C; Collins et al., 2019; Wang et al., 2014; Fig. 13a). These results also match the Tzr calculations of other peralkaline suites in the NaYG province (Fig. 13a). Average Ti-in-zircon geothermometer values range from 786 °C and 684 °C for the Daura and Dutse syenites, 761 °C for the Daura biotite granites, and 783 °C for the Dutse arfvedsonite aegirine granite. The Ti-in-zircon geothermometer values of the Daura-Dutse suites are significantly lower than their zircon saturation temperatures (Supplementary Table S5). This effect has been attributed to the high Zr contents in A-type granites (Schiller and Finger, 2019). The studied granitoids all have high Zr contents (641–1624 ppm), in particular for the Dutse arfvedsonite aegirine granite, therefore the calculated whole-rock Tzr temperatures of the arfvedsonite aegirine granite are considered unreflective of magma crystallization temperature.

Using equations proposed based on total Al contents in biotite (Uchida et al., 2007), the solidification pressures have been estimated for the granitic plutons. For the biotite from the Daura biotite granite, the calculated pressures range from 343 to 405 Mpa (Average – 375 Mpa; Supplementary Table S3) constraining emplacement depths of ~8–10 km (Uchida et al., 2007).

Variations of magma redox can be tracked by variations of Ce<sup>4+</sup>/Ce<sup>3+</sup> and Eu/Eu\* values in zircon (Ballard et al., 2002). For the Daura-Dutse granitoids, zircon Ce<sup>4+</sup>/Ce<sup>3+</sup> and logfO<sub>2</sub> ratios were calculated using a new software (Geo-fO<sub>2</sub>) (Li et al., 2019). The results show overlapping Ce<sup>4+</sup>/Ce<sup>3+</sup> ratios between the Daura amphibole syenite (6–22; average = 11), Daura biotite granite (1–9; average = 6), Dutse fayalite syenite (11–39; average = 15) and Dutse ar-

fvvedsonite aegirine granites (1–32; average = 10) (Fig. 13b–c; Supplementary Table S5), implying a slightly reduced environment during early zircon crystallization. The Daura amphibole syenite and biotite granite primarily plot below the field of the fayalite-magnetite-quartz (FMQ) buffer on a -logfO<sub>2</sub> vs Ti in zircon/°C plot, while, the Dutse fayalite syenite and arfvedsonite aegirine granite largely plot above the FMQ buffer (Fig. 13d). This suggests reduced conditions for the emplacement of the Daura amphibole syenite and biotite granite with slightly reduced to oxidized conditions for the Dutse fayalite syenite and the Dutse arfvedsonite aegirine granites. In addition, clinopyroxene composition from the Daura and Dutse syenites trend towards Hed-rich end members overlapping with the evolutionary trends noted in pyroxenes from the North Quroq alkaline suites, South Greenland, also indicating a relatively reduced magma (Fig. 5b; trend (6);  $\Delta$ FMQ = −0.5 to −3; Marks et al., 2008). Indeed, the slightly reduced oxygen fugacity values for the Daura-Dutse granitoids is typical for mantle-derived A<sub>1</sub>-type granites (−5 to + 0.5; Dall'Agnol and Oliveira, 2007; Wang et al., 2018b).

#### 5.5. Trigger mechanism for emplacement episodes in the Niger-Nigeria alkaline granite province

The temporospatial distribution of alkaline magmatic centres in the Niger-Nigeria alkaline province is a prominent geological feature that has attracted much attention (Black et al., 1985; Ngako et al., 2006). The dynamic mechanism driving the emplacement of the alkaline magmatism in the province likely triggered involvement of deep mantle materials (Girei et al., 2019). However, the region during this period (470–141 Ma) is not associated with any orogenic movement in West Africa suggesting an anorogenic setting. Several workers have suggested the existence of a mantle plume beneath the West African plate during time periods overlapping the emplacement period of the Niger-Nigeria A-type granites (Morgan, 1981; Rahaman et al., 1984). This has led to other workers to propose plate migration over a mantle plume for the north to south age migration trend in the Niger-Nigeria alkaline province (Bowden et al., 1976; Kamaunji et al., 2020).

However, several unique features of the Niger-Nigeria alkaline province are incompatible with a mantle plume model. Firstly, the anorogenic complexes are emplaced along a relatively narrow longitudinal band (50–100 km). This is in contrast to plume generated “hot spot” tracks where a wider base area (> 500 km) is affected by hotspot melting (Shellnutt et al., 2009). Secondly, the temporospatial distribution of anorogenic magmatic centres in the Niger-Nigeria province show distribution of these centres along E-W, ENE-WSW, and NNW-SSE transcurrent faults (Fig. 10b–d) which are spatially related to the a large regional N-S-trending Raghane shear structure that stretches from Hoggar region in North Africa (Fig. 1a). The deviation of some alkaline complexes from the general N-S trend (Fig. 10a–c) could be attributed to the emplacement along secondary transcurrent fault systems (Black et al., 1985). Thirdly, the calculated migratory rates of the northern NrYG (0.5 cm/yr<sup>−1</sup>), southern NrYG to northern NaYG (0.36 cm/yr<sup>−1</sup>) and the northcentral NaYG centres (0.34 cm/yr<sup>−1</sup>) vary significantly (Fig. 10e). These migratory rates are significantly lower than established movement rate for the African plate (0.76 cm/ yr) during this Silurian to Early Cretaceous times and suggest the emplacement of the Niger-Nigeria alkaline suites is unrelated to the migration of the African plate over a mantle plume (Girei et al., 2019; Van Breemen and Bowden, 1973). Fourthly, the 263 Ma porphyritic arfvedsonite aegirine granite along with coeval ~232 Ma fayalite syenite and arfvedsonite aegirine syenite in the Dutse complex establish repeated magmatism in the NaYG province. These repeated emplacement episodes are also inconsistent with the mantle plume model. Furthermore, other geological evidences for the presence of a mantle plume beneath West Africa is lacking.

Structural and seismological evidence suggest reactivations of ancient shear zones within the African plate since Neoproterozoic times (Bailey and Woolley, 2005). These repeated re-activation of regional shear structures since the Neoproterozoic times would have triggered crustal extensional from the Hoggar region down to northcentral Nigeria. The formation and emplacement of the Niger-Nigeria alkaline complexes likely occurred during these periods of reactivation and extension strain. We propose that upwelling of asthenospheric mantle triggered partial melting of lithospheric mantle materials, generating OIB-type mafic melts. Subsequent magma differentiation and crustal contamination of the OIB-like melt result in the formation of felsic peralkaline syenitic and granitic magmas (Fig. 15a–c). Reactivations of ancient shear zones triggered regional extension, which induced pressure releasing and arising of the peralkaline magmas. During 470–401 Ma, the reactivation and extension started at northern Niger, generating the alkaline-peralkaline rocks in the northern NrYG sub-province (Fig. 15a). Further southward migration of the shear zones and transcurrent faults triggered magmatic emplacements in the southern NrYG and northern NaYG sub-provinces from 330 to 258 Ma (Fig. 15b) and continued with the 263–141 Ma trend seen in the northcentral NaYG sub-province (Fig. 15c).

The reactivation mechanism of these lithospheric shear zones has been linked to abrupt changes in the migratory direction of the African plate during significant events (Bailey and Woolley, 2005). For instance, in the northern NrYG sub-province, Ngako et al. (2006) attributed the emplacement of the ENE-SWS trending complexes to periods of shift in plate motion and accompanied change in the tectonic stress field. They surmised that reactivation episodes in the northcentral NaYG sub-province are likely related to the Triassic tectonics associated with the opening of the South Atlantic.

## 6. Conclusions

In northern Nigeria, the Daura and Dutse alkaline suites show atypical geochemical signatures (depleted CaO and Sr contents, high HFSE, high Ga/Al ratio, etc.) synonymous with A<sub>1</sub>-type (alkaline and anorogenic) granite. Based on textural, geochemical and isotopic data, the Daura amphibole syenites were likely generated by crystal accumulation of residual silicic liquid during cooling with limited crustal contamination, while, the Dutse syenites were likely derived by fractional crystallization of a slightly reduced mantle-derived melts that also experienced limited crustal contamination. Significant fractional crystallization alongside simultaneous crustal assimilation (AFC) processes led to the formation of the Daura biotite granite and Dutse arfvedsonite granites, respectively. LA-ICPMS zircon U–Pb dating results suggest that the Daura and Dutse suites were mainly emplaced between 324 and 322 and 263–232 Ma, respectively. These new ages constrain the onset time of anorogenic alkaline magmatism in the NaYG as a Late Carboniferous (324 Ma) event, contrary to Late Triassic ages (213 Ma) reported by other workers. The zircon age of the Daura complex is well linked with the age of the Zinder complex (~330 Ma) in the southernmost NrYG province, reflecting a continuous emplacement chain between the NrYG and NaYG provinces. Overall, an N-S trend is apparent for the Nigerian alkaline granite province with subordinate emplacement along E-W and NW-SE trends. We propose that the reactivation of transcurrent fault systems is likely the primary mechanism for the formation of the Niger-Nigeria alkaline granite province and can account for the apparent “age migration” in the Niger-Nigeria alkaline belt.

Supplementary data to this article can be found online at <https://doi.org/10.1016/j.lithos.2021.106561>.

## Uncited reference

### Declaration of Competing Interest

The authors declare that they have no known competing financial interests or personal relationships that could have appeared to influence the work reported in this paper.

### Acknowledgement

The National Nature Science Foundation of China (No. 42072082), the Open Fund of the Research Center for Petrogenesis and Mineralization of Granitoid Rocks, China Geological Survey (PMGR202001) and the China Geological Survey Project (DD20201152) financially supported this work. We thank Dr. Greg Shellnutt for his editorial handling of this submission as well as two anonymous reviewers for their constructive comments and suggestions that greatly improved this manuscript.

### References

- Ahmed, H.A., Wang, L.-X., Ma, C.-Q., Abdalsamed, M.I., Girei, M.B., Zhu, Y.-X., Vincent, V.I., Kamaunji, D.V., Cao, L., 2021. Contrasting Neoproterozoic and Mesozoic granitoids in Zaranda complex (Nigeria): insights into the distinct origins, tectonic settings and mineralization potential. *Int. J. Earth Sci.* 1–25.
- Amuda, A.K., Yang, X., Deng, J., Faisal, M., Cao, J., Bute, S.I., Girei, M.B., Elatikpo, S.M., 2020. Petrogenesis of the peralkaline Dutsen Wai and Ropp complexes in the Nigerian younger granites: implications for crucial metal enrichments. *Int. Geol. Rev.* 1–25.
- Bailey, D.K., Woolley, A.R., 2005. Repeated synchronous magmatism within Africa: timing, magnetic reversals, and global tectonics. In: Foulger, G.R., Natland, J.H., Presnall, D.C., Anderson, D.L. (Eds.), *Plates, Plumes and Paradigms: Geological Society of America, Special Paper*, 388, pp. 365–377.
- Ballard, J.R., Palin, M.J., Campbell, I.H., 2002. Relative oxidation states of magmas inferred from Ce(IV)/Ce(III) in zircon: application to porphyry copper deposits of northern Chile. *Contrib. Mineral. Petrol.* 144, 347–364.
- Ballmer, M.D., Conrad, C.P., Smith, E.I., Harmon, N., 2013. Non-hotspot volcano chains produced by migration of shear-driven upwelling toward the East Pacific rise. *Geology* 41 (4), 479–482.
- Batchelor, R.A., Bowden, P., 1986. Major and Trace Element Analysis of Volcanic and Sub-Volcanic Igneous Rocks for the Nigerian-Niger Anorogenic Complex. Overseas Development Administration Research Scheme, R2679, 33p.
- Bennett, J.N., Turner, D.C., Ike, E.C., Bowden, P., 1984. The geology of the northern Nigerian anorogenic ring-complexes. *Overs. Geol. Miner. Res.* 61, 1–60.
- Black, R., Lameyre, J., Bonin, B., 1985. The structural setting of alkaline complexes. *J. Afr. Earth Sci.* 3, 5–16.
- Bowden, P., 1985. The geochemistry and mineralization of alkaline ring complexes in Africa (a review). *J. Afr. Earth Sci.* 3, 17–39.
- Bowden, P., Van Breemen, O., Hutchison, J., Turner, D.C., 1976. Palaeozoic and Mesozoic age trends for some ring complexes in Nigeria and Niger. *Nature* 1 (259), 297–299.
- Bowden, P., Black, R., Martin, I.F., Ike, I.C., Kinnaird, J.A., Batchelor, R.A., 1987. Nigerian alkaline ring-complexes: a classical example of African Phanerozoic anorogenic told-plate magmatism. In: Flton, J.G., Upton, B.J.G. (Eds.), *Alkaline Igneous Rocks*, 30. *Geol. Soc. Spec. Publ.*, pp. 357–379.
- Bute, S.I., Yang, X., Cao, J., Liu, L., Deng, J., Vela Haruna, I., Girei, M.B., Abubakar, U., Akhtar, S., 2019. Origin and tectonic implications of ferroan alkali-calcic granitoids from the Hawal Massif, east-eastern Nigeria terrane: clues from geochemistry and zircon U-Pb-Hf isotopes. *Int. Geol. Rev.* 62, 129–152.
- Collins, W.J., Huang, H.Q., Bowden, P., Kemp, A.I.S., 2019. Repeated S-I-A-Type Granite Trilogy in the Lachlan Orogen, and Geochemical Contrasts with A-Type Granites in Nigeria: Implications for Petrogenesis and Tectonic Discrimination. *Geological Society of London Collection*.
- Coulson, I.M., 2003. Evolution of the North Qoroq Centre nepheline syenites, South Greenland: alkali-mafic silicates and the role of metasomatism. *Mineral. Mag.* 67, 873–892.
- Dall'Agnol, R., Oliveira, D.C., 2007. Oxidized, magnetite-series, rapakivi-type granites of Carajás, Brazil: implications for classification and petrogenesis of A-type granites. *Lithos* 93, 215–233.
- De la Roche, H., Leterrier, J., Grandclaude, P., Marchal, M., 1980. A classification of volcanic and plutonic rocks using R1R2-diagrams and major element analysis—its relationships with current nomenclature. *Chem. Geol.* 29, 183–210.
- Demaiffe, D., Moreau, C., Brown, W.L., Weis, D., 1991. Geochemical and isotopic (Sr, Nd and Pb) evidence on the origin of the anorthosite bearing anorogenic complexes of the Air province, Niger. *Earth Planet. Sci. Lett.* 105, 28–46.
- Dickin, A.P., Halliday, A.N., Bowden, P., 1991. A Pb, Sr and Nd isotope study of the basement and mesozoic ring complexes of the Jos Plateau, Nigeria. *Chem. Geol.* 94, 23–32.
- Ebinger, C., 2005. Continental breakup: the East African perspective. *Astron. Geophys.* 46, 2.16–2.21.
- Eby, G.N., 1990. The A-type granitoids: a review of their occurrence and chemical

- characteristics and speculations on their petrogenesis. *Lithos* 26, 115–134.
- Eby, G.N., 1992. Chemical subdivision of the A-type granitoids: petrogenetic and tectonic implications. *Geology* 20, 641–644.
- Foster, M.D., 1960. Interpretation of the composition of trioctahedral micas. US Geol. Surv. Prof. Pap. B, 354, 1–49.
- Frost, C.D., Frost, B.R., 2001. On ferroan (A-type) granitoids: their compositional variability and modes of origin. *J. Petrol.* 52, 39–53.
- Ganade, C.E., Cordani, U.G., Agbossoumouende, Y., Caby, R., Basei, M.A., Weinberg, R.F., Sato, K., 2016. Tightening-up NE Brazil and NW Africa connections: new U-Pb/Lu-Hf zircon data of a complete plate tectonic cycle in the Dahomey belt of the West Gondwana Orogen in Togo and Benin. *Precambrian Res.* 276, 24–42.
- Gervasoni, F., Klemme, S., Rocha-Júnior, E.R., Berndt, J., 2016. Zircon saturation in silicate melts: a new and improved model for aluminous and alkaline melts. *Contrib. Mineral. Petro.* 171 (3), 1–12.
- Girei, M.B., Li, H., Algeo, T.J., Bonin, B., Ogunkoye, P.O., Bute, S.I., Ahmed, H.A., 2019. Petrogenesis of A-type granites associated with Sn–Nb–Zn mineralization in Ririwei complex, north-central Nigeria: constraints from whole-rock Sm–Nd and zircon Lu–Hf isotope systematics. *Lithos* 340–341, 49–70.
- Girei, M.B., Li, H., Vincent, V.I., Algeo, T.J., Elatikpo, S.M., Bute, S.I., Ahmed, H.A., Amuda, A.K., 2020. Genesis and timing of Mo mineralization in the Mada Ring complex, north-central Nigeria: insights from whole-rock geochemistry, Nd–Sr isotopes, zircon U–Pb–Hf isotopes, and molybdenite Re–Os systematics. *Mineral. Deposita* 1–20.
- Grange, M., Scharer, U., Merle, R., Girardeau, J., Cornen, G., 2010. Plume–lithosphere interaction during migration of cretaceous alkaline magmatism in SW Portugal: evidence from U–Pb ages and Pb–Sr–Hf isotopes. *J. Petrol.* 51, 1143–1170.
- Green, T.H., 1995. Significance of Nb/Ta as an indicator of geochemical processes in the crust–mantle system. *Chem. Geol.* 120, 347–359.
- Halliday, A.N., Dickin, A.P., Fallackson, A.E., Fifton, J.G., 1988. Mantle dynamics: a Nd, Sr, Pb, and O isotopic study of the Cameroon Line Volcanic Chain. *J. Petrol.* 29, 181–211.
- Hawthorne, F.C., Oberti, R., Harlow, G.E., Maresch, W.V., Martin, R.F., Schumacher, J.C., Welch, M.D., 2012. Nomenclature of the amphibole supergroup. *Am. Mineral.* 97 (11–12), 2031–2048.
- Iizuka, T., Hirata, T., 2005. Improvements of precision and accuracy in situ Hf isotope microanalysis of zircon using the laser ablation-MC-ICPMS technique. *Chem. Geol.* 220, 121–137.
- Jackson, S.E., Pearson, N.J., Griffin, W.L., Belousova, E.A., 2004. The application of laser ablation-inductively coupled plasma-mass spectrometry to in situ U–Pb zircon geochronology. *Chem. Geol.* 211, 47–69.
- Kamaunji, V.D., Wang, L.X., Ahmed, H.A., Zhu, Y.X., Vincent, V.I., Girei, M.B., 2020. Coexisting A1 and A2 granites of Kudaru complex: implications for genetic and tectonic diversity of a-type granite in the Younger Granite province, north-central Nigeria. *Int. J. Earth Sci.* 109, 511–535.
- Karche, J.P., Vachette, M., 1978. Age et migration de l'activité magmatique dans les complexes paleozoïques du Niger, conséquences. *Bull. Soc. Geol. Fr.* 20, 941–953.
- Kinnaird, J.A., 1981. Geology of the Nigerian Anorogenic Ring Complexes. In: Map Scale 1:500,000. John Bartholomew, Edinburgh.
- Kinnaird, J.A., 1985. Hydrothermal alteration and mineralization of the alkaline anorogenic complexes of Nigeria. *J. Afr. Earth Sci.* 3, 229–251.
- Li, W., Cheng, Y., Yang, Z., 2019. Geo-FO(2): integrated software for analysis of magmatic oxygen fugacity. *Geochim. Geophys. Geosyst.* 20, 2542–2555.
- Li, X., Zhang, C., Behrens, H., Holtz, F., 2020a. Experiments on the saturation of fluorite in magmatic systems: implications for maximum F concentration and fluorine-cation bonding in silicate melt. *J. Earth Sci.* 31, 456–467.
- Li, X., Zhang, C., Behrens, H., Holtz, F., 2020b. Calculating amphibole formula from electron microprobe analysis data using a machine learning method based on principal components regression. *Lithos* 362, 105469.
- Liu, Y.S., Hu, Z.C., Gao, S., Gunther, D., Xu, J., Gao, C.G., Chen, H.H., 2008. In Situ analysis of major and trace element of anhydrous minerals by LA-ICP-MS without applying an internal standard. *Chem. Geol.* 257, 34–43.
- Loiselle, M.C., Wones, D.R., 1979. Characteristics and origin of anorogenic granites. In: Abstracts of Papers Presented at the Annual Meetings of the Geological Society of America and Associated Societies. San Diego, California, 11, p. 468.
- Lubala, R., Frick, C., Rogers, J., Walraven, F., 1994. Petrogenesis of syenites and granites of the Schiel Alkaline complex, Northern Transvaal, South Africa. *J. Geol.* 102, 307–316.
- Magaji, S.S., Martin, R.F., Ike, E.C., Ipkonde, A.E., 2011. The Geshere syenite–peralkaline granite pluton: a key to understanding the anorogenic Nigerian Younger Granites and analogues elsewhere. *Period. Mineral.* 80, 199.
- Marks, M.A.W., Schilling, J., Coulson, I.M., Wenzel, T., Markl, G., 2008. The alkaline–peralkaline Tamazeght complex, High Atlas Mountains, Morocco: mineral chemistry and petrological constraints for derivation from a compositionally heterogeneous mantle source. *J. Petrol.* 49, 1097–1131.
- Martin, R.F., 2006. A-type granites of crustal origin ultimately result from open-system fenitization-type reactions in an extensional environment. *Lithos* 91, 125–136.
- Middlemost, E.A.K., 1994. Naming materials in the magma/igneous rock system. *Earth Sci. Rev.* 37, 215–224.
- Moreau, C., Demaiffe, D., Bellion, Y., Boullier, A.-M., 1994. A tectonic model for the location of Palaeozoic ring complexes in Air (Niger, West Africa). *Tectonophysics* 234, 129–146.
- Morgan, W.J., 1981. Hotspot tracks and the opening of the Atlantic and Indian Oceans. In: Emiliani, C. (Ed.), Ideas and Observations on Progress in the Study of the Seas. Wiley, New York, pp. 443–487.
- Morimoto, N., 1988. Nomenclature of pyroxenes. *Mineral. Petrol.* 39 (1), 55–76.
- Nakamura, N., 1974. Determination of REE, Ba, Fe, Mg, Na, and K in carbonaceous and ordinary chondrites. *Geochim. Cosmochim. Acta* 38, 757–775.
- Ngako, V., Njonfang, E., Tongwa, A.F., Affaton, P., Nnange, J.M., 2006. The north-south paleozoic to quaternary trend of alkaline magmatism from Niger-Nigeria to Cameroon: complex interaction between hotspots and Precambrian faults. *J. Afr. Earth Sci.* 45, 241–256.
- Papoutsas, A., Pe-Piper, G., 2014. Geochemical variation of amphiboles in A-type granites as an indicator of complex magmatic systems: Wentworth Pluton, Nova Scotia, Canada. *Chem. Geol.* 384, 120–134.
- Pfander, J.A., Munker, C., Stracke, A., Mezger, K., 2007. Nb/Ta and Zr/Hf in ocean island basalts – implications for crust–mantle differentiation and the fate of Niobium. *Earth Planet. Sci. Lett.* 254, 158–172.
- Rahaman, M.A., Van Breemen, O., Bowden, P., Bennett, J.N., 1984. Age migration of anorogenic ring-complexes in northern Nigeria. *J. Petrol.* 92, 173–184.
- Schiller, D., Finger, F., 2019. Application of Ti-in-zircon thermometry to granite studies: problems and possible solutions. *Contrib. Mineral. Petrol.* 174, 51.
- Shellnutt, J.G., 2021. A cumulate syenite in the upper part of the Honghe-layered mafic-ultramafic intrusion, Emeishan large igneous province, SW China. *Int. J. Earth Sci.* 1–22.
- Shellnutt, J.G., Wang, C.Y., Zhou, M.F., Yang, Y., 2009. Zircon Lu-Hf isotopic compositions of metaluminous and peralkaline A-type granitic plutons of the Emeishan large igneous province (SW China): constraints on the mantle source. *J. Asian Earth Sci.* 35, 45–55.
- Sun, S.S., McDonough, W.F., 1989. Chemical and isotopic systematics of oceanic basalts: Implications for mantle composition and processes. In: Saunders, A.D., Norry, M.J. (Eds.), *Magmatism in the Ocean Basins*, vol. 42. Geological Society of London Special Publication, pp. 313–435.
- Taylor, S.R., McLennan, S.M., 1985. *The Continental Crust: Its Composition and Evolution*. Oxford Press, Blackwell, pp. 1–31.
- Thornton, C.P., Tuttle, O.F., 1960. Chemistry of igneous rocks-[part] 1, Differentiation index. *Am. J. Sci.* 258, 664–684.
- Turner, D.C., Webb, P.K., 1974. The Daura igneous complex, northern Nigeria—a link between the Younger Granite districts of Nigeria and southern Niger. *J. Geol. Soc. Lond.* 130, 71–77.
- Uchida, E., Endo, S., Makino, M., 2007. Relationship between solidification depth of granitic rocks and formation of hydrothermal ore deposits. *Resour. Geol.* 57, 47–56.
- Van Breemen, O., Bowden, P., 1973. Sequential age trends for some Nigerian Mesozoic granites. *Nat. Phys. Sci.* 242, 9–11.
- Van Breemen, O., Hutchinson, J., Bowden, P., 1975. Age and origin of the Nigerian Mesozoic granites: a Rb-Sr isotopic study. *Contrib. Mineral. Petrol.* 50, 157–172.
- Vincent, V.I., Li, H., Girei, M.B., Ahmed, H.A., Ntekim, E.E., 2021. Genesis and age of Pb–Zn mineralization from the Ningi-Bura ring complex, North Central Nigeria: constraints from zircon morphology, U–Pb dating and Lu–Hf isotopes. *Lithos* 106115.
- Vonopartis, L.C., Kinnaird, J.A., Nex, P.A., Robb, L.J., 2021. African A-Type granites: a geochemical review on metallogenetic potential. *Lithos* 106229.
- Wang, L.-X., Marks, M.A.W., Keller, J., Markl, G., 2014. Halogen variations in alkaline rocks from the Upper Rhine Graben (SW Germany): insights into F, Cl and Br behavior during magmatic processes. *Chem. Geol.* 380, 133–144.
- Wang, C., Lu, Y., He, X., Wang, Q., Zhang, J., 2016. The Paleoproterozoic diorite dykes in the southern margin of the North China Craton: insight into rift-related magmatism. *Precambrian Res.* 277, 26–46.
- Wang, L.X., Ma, C.Q., Zhang, C., Zhu, Y.X., Marks, M.A.W., 2018a. Halogen geochemistry of I and A-type granites from Jiuhuashan region (South China): insights into the elevated fluorine in A-type granite. *Chem. Geol.* 478, 164–182.
- Wang, D., Wang, X.L., Cai, Y., Goldstein, S.L., Yang, T., 2018b. Do Hf isotopes in magmatic zircons represent those of their host rocks? *J. Asian Earth Sci.* 154, 202–212.
- Watkins, R.T., le Roex, A.P., 1991. A reinvestigation of the Okenyanya igneous complex: a new geological map, structural interpretation and model of emplacement. *Commun. Geol. Surv. Namibia* 9, 13–22.
- Watson, E.B., Harrison, T., 2005. Zircon thermometer reveals minimum melting conditions on earliest Earth. *Science* 308 (5723), 841–844.
- Wedepohl, K.H., 1995. The composition of the continental crust. *Geochim. Cosmochim. Acta* 59, 1217–1232.
- Wiedenbeck, M., Hanchar, J.M., Peck, W.H., Sylvester, P., Valley, J., Whitehouse, M., Kronz, A., Morishita, Y., Nasdala, L., Fiebig, J., 2004. Further characterisation of the 91500 zircon crystal. *Geostand. Geoanal. Res.* 28, 9–39.
- Wright, J.B., 1969. A simple alkalinity ratio and its application to questions of non-orogenic granite genesis. *Geol. Mag.* 106 (4), 370–384.
- Yang, X.M., Lentz, D.R., 2005. Chemical composition of rock-forming minerals in goldrelated granitoid intrusions, southwestern New Brunswick, Canada: implications for crystallization conditions, volatile exsolution, and fluorine–chlorine activity. *Contrib. Mineral. Petrol.* 150, 287–305.
- Yang, J.-H., Wu, F.-Y., Chung, S.-L., Wilde, S.A., Chu, M.-F., 2006. A hybrid origin for the Qianshan A-type granite, northeast China: geochemical and Sr–Nd–Hf isotopic evidence. *Lithos* 89, 89–106.
- Zhu, Y.X., Wang, L.X., Xiong, Q.H., Ma, C.Q., Zhang, X., Zhang, C., Ahmed, H.A., 2020. Origin and evolution of ultrapotassic intermediate magma: the Songxian syenite massif, Central China. *Lithos* 366.
- Zindler, A., Hart, S., 1986. Chemical geodynamics. *Annu. Rev. Earth Planet. Sci.* 14, 493–571.